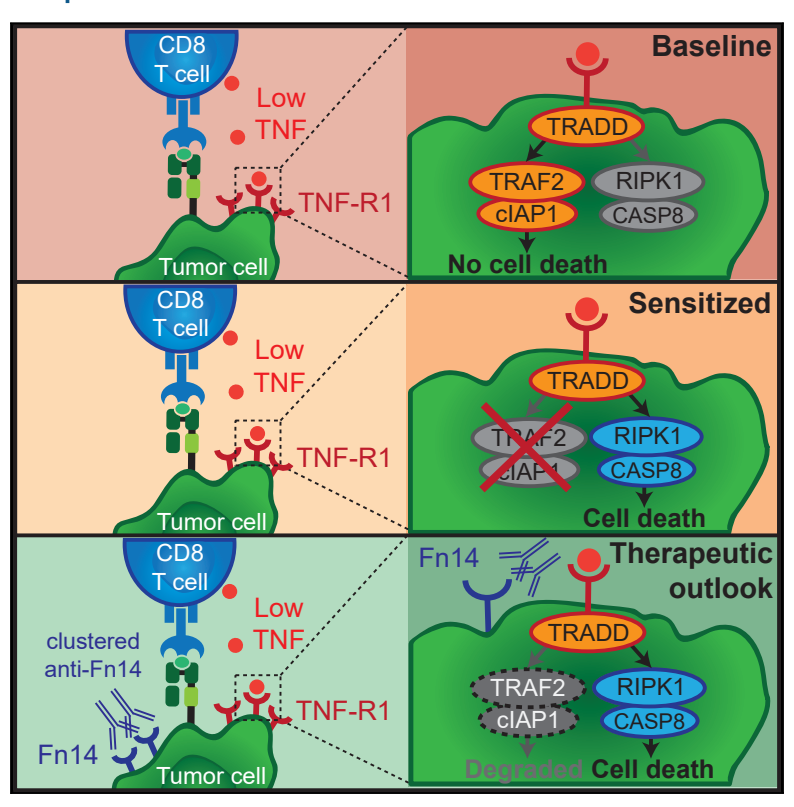
## **Article**



# **Augmenting Immunotherapy Impact by Lowering Tumor TNF Cytotoxicity Threshold**

#### **Graphical Abstract**



#### **Highlights**

- TNF abundance is low in tumors at baseline and in ICB nonresponding patients
- CRISPR/Cas9 screen uncovers hits in the TNF pathway that sensitize to T cell attack
- TRAF2 inactivation lowers tumor cytotoxicity threshold to T cell-derived TNF
- Combined targeting of TRAF2/cIAP1 increases ICB impact

#### **Authors**

David W. Vredevoogd, Thomas Kuilman, Maarten A. Ligtenberg, ..., Maarten Altelaar, Ton N. Schumacher, Daniel S. Peeper

### Correspondence

d.peeper@nki.nl

#### In Brief

New opportunities are needed to increase immune checkpoint blockade (ICB) impact for cancer patients. A genomewide CRISPR/Cas9 screen uncovered several hits in the TNF pathway sensitizing tumor cells to T cell elimination. TNF antitumor activity was generally limited in tumors at baseline and in ICB non-responders, correlating with its low abundance. Selective inactivation of TNF signaling lowered melanoma and lung cancer thresholds to low TNF levels, thereby increasing tumor susceptibility to T cell attack and augmenting benefit from anti-PD-1 treatment.





## **Article**

# Augmenting Immunotherapy Impact by Lowering Tumor TNF Cytotoxicity Threshold

David W. Vredevoogd,<sup>1,6</sup> Thomas Kuilman,<sup>1,6,7</sup> Maarten A. Ligtenberg,<sup>1</sup> Julia Boshuizen,<sup>1</sup> Kelly E. Stecker,<sup>5</sup> Beaunelle de Bruijn,<sup>1</sup> Oscar Krijgsman,<sup>1</sup> Xinyao Huang,<sup>1</sup> Juliana C.N. Kenski,<sup>1</sup> Ruben Lacroix,<sup>1</sup> Riccardo Mezzadra,<sup>1</sup> Raquel Gomez-Eerland,<sup>1</sup> Mete Yildiz,<sup>1</sup> Ilknur Dagidir,<sup>1</sup> Georgi Apriamashvili,<sup>1</sup> Nordin Zandhuis,<sup>1</sup> Vincent van der Noort,<sup>2</sup> Nils L. Visser,<sup>1</sup> Christian U. Blank,<sup>3</sup> Maarten Altelaar,<sup>4,5</sup> Ton N. Schumacher,<sup>1</sup> and Daniel S. Peeper<sup>1,8,\*</sup>

<sup>1</sup>Division of Molecular Oncology and Immunology, Oncode Institute, Netherlands Cancer Institute, Plesmanlaan 121, 1066 CX, Amsterdam, the Netherlands

https://doi.org/10.1016/j.cell.2019.06.014

#### **SUMMARY**

New opportunities are needed to increase immune checkpoint blockade (ICB) benefit. Whereas the interferon (IFN) $\gamma$  pathway harbors both ICB resistance factors and therapeutic opportunities, this has not been systematically investigated for IFN<sub>γ</sub>-independent signaling routes. A genome-wide CRISPR/Cas9 screen to sensitize IFNy receptor-deficient tumor cells to CD8 T cell elimination uncovered several hits mapping to the tumor necrosis factor (TNF) pathway. Clinically, we show that TNF antitumor activity is only limited in tumors at baseline and in ICB non-responders, correlating with its low abundance. Taking advantage of the genetic screen, we demonstrate that ablation of the top hit, TRAF2, lowers the TNF cytotoxicity threshold in tumors by redirecting TNF signaling to favor RIPK1-dependent apoptosis. TRAF2 loss greatly enhanced the therapeutic potential of pharmacologic inhibition of its interaction partner cIAP, another screen hit, thereby cooperating with ICB. Our results suggest that selective reduction of the TNF cytotoxicity threshold increases the susceptibility of tumors to immunotherapy.

#### INTRODUCTION

Clinical strategies unleashing T cell cytotoxicity have significantly improved the perspective of cancer patients (Borghaei et al., 2015; Hodi et al., 2010; Larkin et al., 2015; Motzer et al., 2015; Robert et al., 2011; Rosenberg et al., 2016; Wolchok et al., 2017). By immune checkpoint blockade (ICB), particularly PD-1, PD-L1, or CTLA-4, T cells can be functionally reinvigorated to respond to their cognate antigens (Ahmadzadeh et al., 2009;

Barber et al., 2006; Freeman et al., 2000; Leach et al., 1996). Renewed activity of CD8 T cells is accompanied by increased proliferation, cytokine production, and cytolytic activity (Barber et al., 2006; Freeman et al., 2000; Jacquelot et al., 2017), allowing for efficient immune clearance (Chen and Mellman, 2017; Ji et al., 2012). However, for various reasons, including intrinsic and adaptive tumor resistance, most patients do not benefit durably (Borghaei et al., 2015; Curiel et al., 2004; Dong et al., 2002; Hodi et al., 2010; Larkin et al., 2015; Motzer et al., 2015; Peng et al., 2015; Robert et al., 2011; Rosenberg et al., 2016; Sharma et al., 2017; Wolchok et al., 2017), emphasizing the need for additional, novel therapeutic targets.

Most current immunotherapeutic approaches serve to improve T cell function and leverage their activity (Ahmadzadeh et al., 2009; Barber et al., 2006; Freeman et al., 2000; Leach et al., 1996). Whereas active cytotoxic T cells are a prerequisite for a successful immune response, increasing the susceptibility of tumor cells to T cell-derived death signals may act as an effective and complementary immunotherapeutic strategy. Cytokines such as interferon (IFN)γ, tumor necrosis factor (TNF), Fas, and TNF-related apoptosis-inducing ligand (TRAIL) contribute to the antitumor activity of cytotoxic T cells by inducing proliferative arrest and/or apoptosis (Barber et al., 2006; Barth et al., 1991; Benci et al., 2016; Brincks et al., 2008; Gao et al., 2016; Kearney et al., 2017, 2018). While defects in the IFNγ pathway in tumors correlate with resistance to ICB (Gao et al., 2016; Shin et al., 2017; Zaretsky et al., 2016), modulation of specific factors in this pathway can improve antitumor immune response (Manguso et al., 2017; Pan et al., 2018; Patel et al., 2017). These observations underscore the importance of a thorough understanding of the cell-intrinsic mechanisms that determine a tumor's susceptibility to T cell antitumor activity, as this may open new avenues for therapeutic intervention.

Whereas it is well established that cytokines other than IFN $\gamma$  contribute to T cell cytotoxicity (Barber et al., 2006; Barth et al., 1991; Benci et al., 2016; Brincks et al., 2008; Gao et al.,



<sup>&</sup>lt;sup>2</sup>Division of Statistics, Netherlands Cancer Institute, Plesmanlaan 121, 1066 CX, Amsterdam, the Netherlands

<sup>&</sup>lt;sup>3</sup>Division of Medical Oncology, Netherlands Cancer Institute, Plesmanlaan 121, 1066 CX, Amsterdam, the Netherlands

<sup>&</sup>lt;sup>4</sup>Proteomics Facility, Netherlands Cancer Institute, Plesmanlaan 121, 1066 CX, Amsterdam, the Netherlands

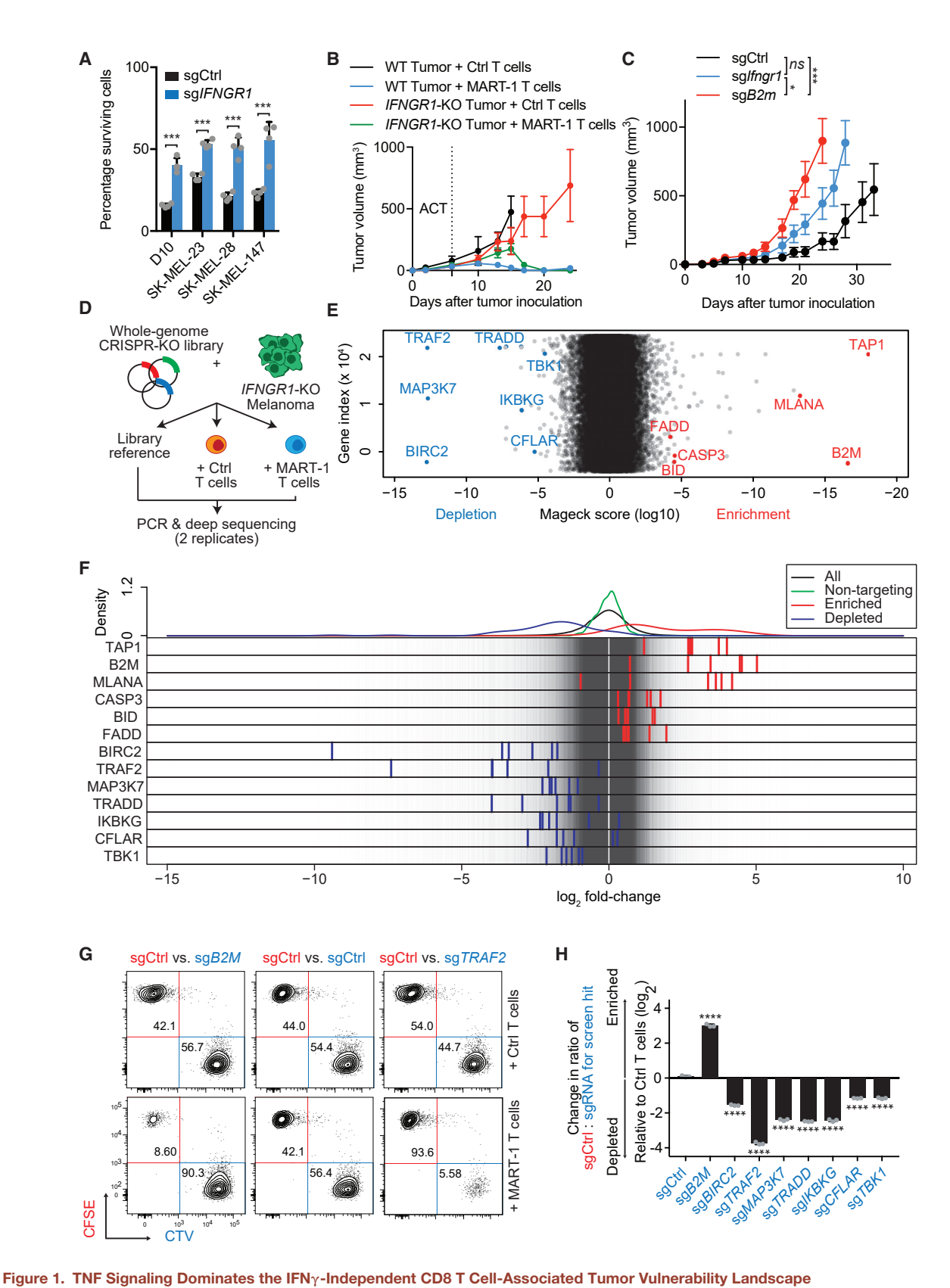
<sup>&</sup>lt;sup>5</sup>Biomolecular Mass Spectrometry and Proteomics, Center for Biomolecular Research and Utrecht Institute for Pharmaceutical Sciences, Utrecht University, Padualaan 8, 3584 CH, Utrecht, the Netherlands

<sup>&</sup>lt;sup>6</sup>These authors contributed equally

<sup>&</sup>lt;sup>7</sup>Present address: Neogene Therapeutics, Matrix VII, Science Park 106, 1098 XG, Amsterdam, the Netherland

<sup>&</sup>lt;sup>8</sup>Lead Contact

<sup>\*</sup>Correspondence: d.peeper@nki.nl



(A) Quantification of T cell cytotoxicity assays of the indicated *IFNGR1*-proficient and *IFNGR1*-deficient human melanoma cell lines after exposure to MART-1 T cells at a 1:2 ratio for all cell lines. Error bars indicate SD. Representative of 3 experiments, each n = 4.

(legend continued on next page)

2016; Ji et al., 2012; Kakaradov et al., 2017; Kearney et al., 2017; Zhang et al., 2015), IFN $\gamma$ -independent tumor signaling pathways have not yet been explored in a systematic and unbiased fashion for new therapeutic targets. Therefore, we set out to integrate genome-wide CRISPR-Cas9 screening in paired T cell: IFN $\gamma$  receptor (IFNGR1)-deficient tumor systems with analyses of immunotherapy-treated patients to provide a functional and clinically meaningful annotation of the IFN $\gamma$ -independent, T cell-associated tumor vulnerability landscape.

#### **RESULTS**

## Cytotoxic Potential of IFN $\gamma$ -Independent CD8 T Cell Signaling Modalities

Given the established antitumor activity of T cell cytokines other than IFN $\gamma$  (Kearney et al., 2017; Schulze-Osthoff et al., 1998), we first experimentally queried the relative contribution of IFN $\gamma$  to T cell-mediated tumor killing. We challenged a matched panel of either IFNGR1 wild type (WT) or IFNGR1 knockout (KO) human HLA-A\*02:01\*/MART1\* melanoma cell lines *in vitro* with healthy donor CD8 T cells, which had been retrovirally transduced with a MART-1-specific T cell receptor (MART-1 T cells) (Gomez-Eerland et al., 2014). Even though IFN $\gamma$  signaling was disabled, these *IFNGR1*-KO cell lines remained remarkably susceptible to T cell killing when challenged *in vitro* (Figures 1A, S1A, and S1B).

This result was corroborated in vivo, in a NOD severe combined immunodeficiency (SCID) gamma/B2m-deficient (NSG) mouse model, in which either parental or IFNGR1-deficient human melanoma cell lines were grafted, followed by adoptive cell transfer (ACT) with human control T cells or MART-1 T cells. IFNGR1-KO tumors strongly regressed upon adoptive cell transfer, albeit in a delayed fashion compared to their parental counterparts (Figure 1B). To assess the role of IFN $\gamma$  in immune-competent, tumor-bearing C57BL/6 mice, we used the murine Braf<sup>V600E</sup>:Pten<sup>-/-</sup> melanoma cell line D4M.3A (Jenkins et al., 2014) expressing the model antigen ovalbumin (OVA). Compared to control tumors, Ifngr1-knockout tumors partially escaped immune control, but significantly less so than B2m-deficient tumors which, due to their lack of antigen presentation, are fully exempt from CD8 T cell attack (Figure 1C). The results from these three independent experiments demonstrate a significant contribution of IFN<sub>γ</sub>-independent signaling to T cell antitumor activity, thereby highlighting the potential of also therapeutically exploiting IFNγ-independent T cell activity.

## Genome-wide CRISPR-Cas9 Screen for IFNγ-Independent Tumor Factors Increasing T Cell Sensitivity

To genetically define the IFN<sub>γ</sub>-independent genetic tumor landscape, we set out to identify therapeutic targets that upon inactivation increase tumor susceptibility to T cell elimination. Prompted by the results described above, we performed an unbiased genome-wide CRISPR-Cas9 knockout screen in IFNGR1-deficient melanoma cells (Figure 1D). Cells were infected in duplicate with the GeCKO library (Shalem et al., 2014) and challenged with MART-1 T cells derived from independent healthy individuals to circumvent donor-specific effects. Surviving melanoma cells were collected, and single guide RNAs (sgRNAs) were amplified from their genomic DNA by PCR and analyzed by deep sequencing (Table S1). We observed a strong correlation between the replicates (Figure S1C). Moreover, essential genes were selectively depleted as expected (Figure S1D). Further illustrating the robustness of the screen, sgRNAs targeting the antigen presentation machinery (B2M, TAP1), or the antigen itself (MLANA), conferred resistance to T cell killing (Figure 1E, F), which was confirmed by gene set enrichment analysis (GSEA) (Figure S1E; Table S2).

At the other end of the spectrum, we identified several sgRNAs that, instead, strongly sensitized tumor cells to T cell elimination (Figures 1E and 1F). The two most significantly depleted genes were TNF receptor-associated factor 2 (TRAF2) and BIRC2 (encoding cellular Inhibitor of apoptosis 1 [cIAP1]). Interestingly, the former is known to recruit the latter to inhibit death receptor-mediated apoptosis (Hsu et al., 1996; Mahoney et al., 2008; Shu et al., 1996; Wang et al., 1998; Yeh et al., 1997). While TRADD, another hit, is implicated in T cell- and TNF-induced apoptosis, its loss also sensitizes to T cell-derived TRAIL (Cao et al., 2011; Kearney et al., 2018; Kim et al., 2011). Other hits included MAP3K7, IKBKG, CFLAR, and TBK1. GSEA showed that a TNF pathway, but not an IFN $\gamma$  pathway, gene set was enriched among sensitizing hits (Figure S1E; Table S2).

To validate the screen hits, cells were transduced with individual sgRNA hits (labeled violet, Table S7), mixed 1:1 with sgCtrl-transduced ones (labeled green) and used in a competitive T cell cytotoxicity assay. Flow cytometric analysis validated all

<sup>(</sup>B) In vivo growth of IFNGR1-proficient and IFNGR1-deficient D10 human melanoma clones after adoptive cell transfer (ACT) of untransduced (control) CD8 T cells or MART-1 CD8 T cells in an NSG murine xenograft model. Error bars indicate SEM; n = 4 mice per group.

<sup>(</sup>C) In vivo growth in C57BL/6 mice of D4M.3A-OVA murine melanoma cell lines harboring either sglfngr1, sgB2m or a non-targeting control sgRNA. Error bars indicate SEM; n = 10 mice per group. Significance was determined at day 24 using an ANOVA test with Tukey post hoc testing.

<sup>(</sup>D) Schematic overview of CRISPR-Cas9 knockout screen in IFNGR1-deficient D10 human melanoma cells.

<sup>(</sup>E) Log<sub>10</sub>-transformed MAGeCK robust ranking aggregation (RRA)-scores for either depletion (left) or enrichment (right) of sgRNAs in tumor cells challenged with MART-1 T cells versus control T cells.

<sup>(</sup>F) Log<sub>2</sub>-fold change of the individual sgRNAs counts (MART-1 T cells versus control T cells) targeting the genes identified in (E). sgRNAs targeting enriched and depleted genes are demarcated in red and blue, respectively.

<sup>(</sup>G) Competition assays of melanoma cells expressing sgRNAs as indicated upon control or MART-1 T cell challenge. Representative flow cytometry plots are shown (n = 3).

<sup>(</sup>H) Quantification of the data in (G) and all other targeted genes. The change in ratio of a sgRNA targeting a hit versus sgCtrl is represented relative to melanoma cells challenged with control T cells ( $log_2$ ). Grey dots represent individual measurements (n = 3), and error bars indicate SD. \*p < 0.05; \*\*p < 0.01; \*\*\*p < 0.001; \*\*\*\*p < 0.001, \*\*\*\*\*\*\*p < 0.0001.

See also Figure S1 and Tables S1, S2, and S7.

screen hits tested (Figures 1G and 1H), and this was confirmed in non-competitive cytotoxicity assays and with independent *IFNGR1*-KO clones (Figures S1F–S1I). For the remainder of this study, we focused on our top hit, TRAF2. Its depletion increased tumor sensitivity to T cell killing independently of IFN $\gamma$  signaling, and this was rescued by TRAF2 reconstitution (Figures S1J and S1K). Thus, this genome-wide screen yielded a series of confirmed IFN $\gamma$  signaling-independent hits, depletion of which strongly sensitizes tumor cells to T cell killing. These results demonstrate that the TNF pathway can be functionally mined to yield critical factors determining the susceptibility of tumors to T cell elimination.

#### Highly Conserved Engagement of TNF Signaling Pathway upon Tumor Engagement by T Cells

We next evaluated the role of TNF in driving an effective anti-tumor immune response, with transcriptomic analysis and in clinical samples. To define the transcriptional changes upon T cell challenge, we subjected a panel of melanoma cell lines and cognate MART-1 T cells to RNA sequencing after 0, 4, and 14 hours of co-culturing. By unbiased computational filtering, we found that out of 79 human cytokines, 43 were transcriptionally induced in T cells upon engagement with tumor cells (Figures S2A and S2B; Table S3). Cognate receptors were expressed for ten and four of those induced an actual response signature by GSEA, namely IFN $\gamma$ , transforming growth factor  $\beta$  (TGF- $\beta$ ), TNF, and TRAIL (Figures S2C and S2D; Tables S2, S3, and S4). We also confirmed the engagement of the TNF signaling pathway at the protein level by a proteomics-based approach (Figure S2E; Table S5). The engagement of these cytokine signaling pathways was further recapitulated in tumors of melanoma patients, showing concordance between the presence of activated CD8 T cells and these cytokine-related gene signatures, including TNF (Figure S2F). These results indicate that the engagement of TNF signaling pathway upon tumor: T cell encounter is a conserved trait that is also observed in patients' tumors.

## Important Role for TNF in ICB-Responding Tumors but Not in Untreated Tumors

We next wished to obtain clinical substantiation of these results and investigated a possible role for T cell-derived TNF in functionally affecting patient tumors. In The Cancer Genome Atlas (TCGA) analysis (comprising pre-treatment tumors), we generally did not detect a correlation between TNF expression and patient survival (Figure 2A). As a complementary approach, we assessed whether the TNF signaling pathway in tumors is subject to selective mutational pressure by the immune system, as has been described for IFNγ signaling (Gao et al., 2016; Sharma et al., 2017; Shin et al., 2017; Zaretsky et al., 2016). We could not find a correlation between non-synonymous TNF pathway mutations and survival in any cancer subtype (Figure 2B). Together, these data suggest that under baseline conditions, TNF is unlikely to act as a potent tumor cytotoxic factor, and it is necessary, but not sufficient, for anti-tumor effects. We corroborated this notion in vitro: in a dose-titration experiment, even high concentrations of TNF were not cytotoxic (Figure 2C; and see below).

Because ICB increases cytokine production (Jacquelot et al., 2017), we next analyzed tumor gene expression data of two patient cohorts treated with anti-PD-1 (Riaz et al., 2017; Roh et al., 2017). We hypothesized that any clinical role of TNF in T cell antitumor activity may be unleashed by ICB, particularly in responding patients. Supporting this idea, in both cohorts we detected higher expression of TNF in responding patients (R) than in non-responding ones (NR), but only after therapy onset (Figures 2D and S2G). The higher expression levels of TNF were corroborated by a similar increase of a TNF response signature in both datasets (Figures 2E and S2H). Such correlations were also observed for an IFN $_{\Upsilon}$  signature (Ayers et al., 2017) (Figures S2I and S2J).

This led us to hypothesize that the rise in TNF levels upon ICB response drives tumor cytotoxicity. We performed a complementary analysis in which we again assessed selective mutational pressure by TNF on the TNF signaling pathway as a whole, but this time comparing tumor mutations before and after onset of therapy. This revealed that both response duration and overall survival were profoundly lower for treated patients with tumors harboring non-synonymous TNF pathway mutations than WT TNF pathway tumors (Figures 2F and 2G; Table S6). These included several dozen mutations in established and essential signaling proteins in the TNF pathway, such as RIPK1, NFKB1, CYLD, and the protein MADD; a key transducer of TNF-mediated prosurvival signals (Kurada et al., 2009; Schievella et al., 1997). This association remained when we assessed TNF pathway mutations specifically predicted to negatively affect protein function (Figure S2K). Future functional studies will be required to determine the individual impact of all these mutations on TNF pathway signaling output. In a second patient cohort, with limited followup of patient survival, we detected a similar trend (Figure S2L). These correlations could not be found for IFN $\gamma$  pathway mutant tumors (Figures S2M and S2N). Collectively, these data imply that in ICB-responding tumors, but not under baseline conditions. TNF plays a crucial role: because its expression rises with ICB response, this sets the stage for immune editing of the TNF pathway, causing reduced ICB responsiveness.

#### **TRAF2** Inactivation Reduces TNF Cytotoxicity Threshold

These clinical data suggest an important role of TNF in driving an antitumor response in the context of ICB. Another implication of these results is that in untreated tumors, and those unresponsive to ICB, there is a low abundance of TNF, which is insufficient to exert meaningful antitumor activity. Therefore, we argued that for tumors at baseline to become susceptible to T cell elimination, the threshold to respond to TNF would need to be lowered. Taking advantage of the CRISPR/Cas9 screen results, we hypothesized that this can be achieved by inactivating the tumor-intrinsic TNF pathway. Specifically, we assessed whether inactivation of TRAF2, the top hit in the screen, sensitizes tumors to low concentrations of TNF. In contrast to WT cells, which hardly displayed any sensitivity to TNF, TRAF2 inactivation dramatically reduced the TNF cytotoxicity threshold, to the extent that tumor cells died at picogram TNF concentrations (Figure 2C). Such concentrations are physiologically relevant, since they were found in both tumor samples and patient serum analyses (Sasi et al., 2012; Yurkovetsky et al., 2007). These results are in line

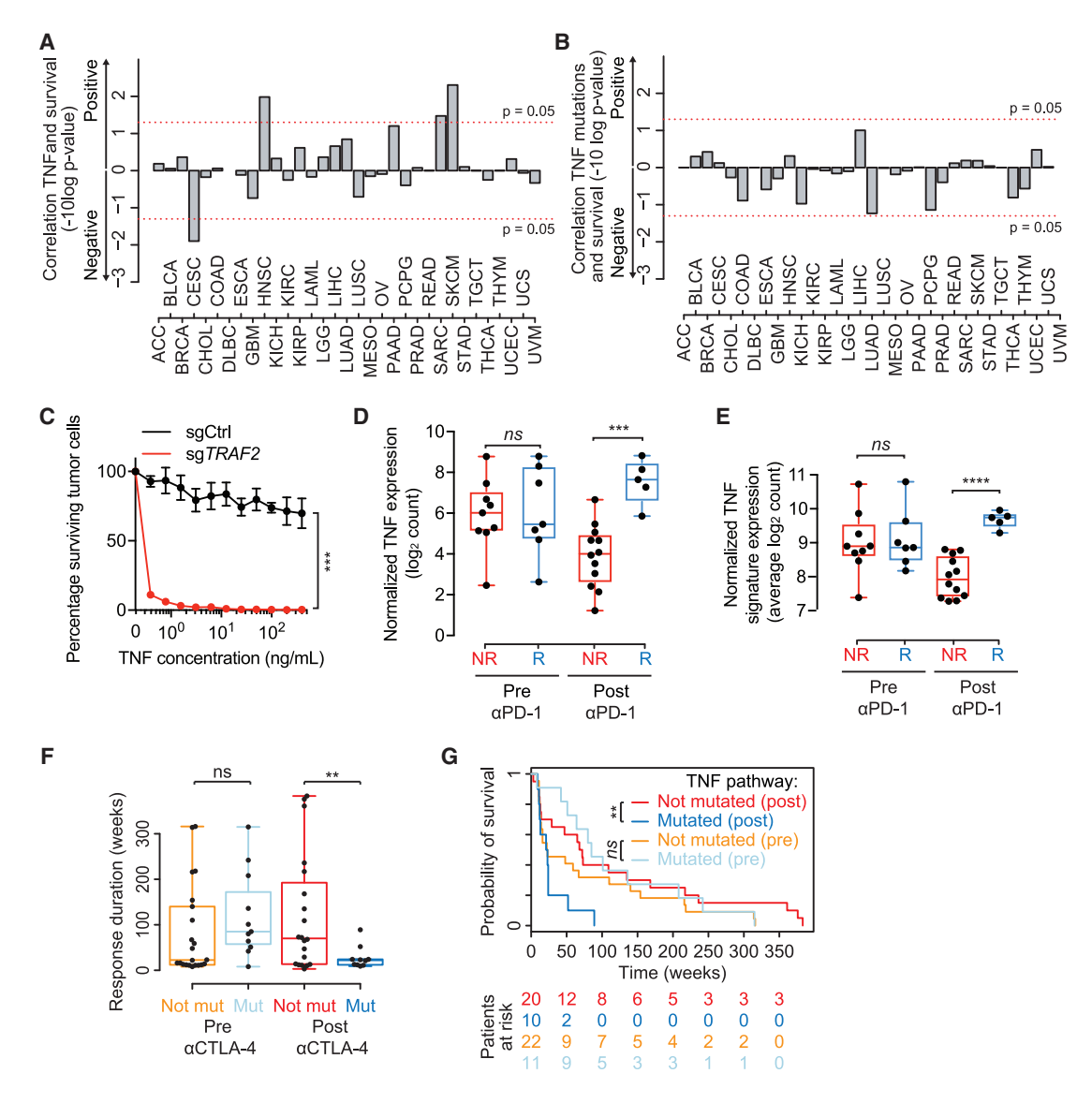


Figure 2. Important Role for TNF in ICB-Responding Tumors but Not in Untreated Tumors

- (A) Correlation between TNF expression and survival in TCGA. The y axis represents a signed -log10(p value) of the correlation between TNF expression (1<sup>st</sup> versus 4<sup>th</sup> quartile) and survival (log-rank test; see STAR Methods).
- (B) Correlation between TNF pathway mutational status and survival in TCGA. The y axis represents a signed -log10(p value) of the correlation between TNF pathway mutational status and survival (log-rank test; see STAR Methods).
- (C) Quantification of surviving sgCtrl or sgTRAF2 melanoma cells after TNF treatment at indicated concentrations (representative of three individual experiments, each n = 3). Results were significant at all tested concentrations, as determined by multiple Student's t tests and Bonferroni multiple testing correction. Error bars indicate SD.
- (D) Normalized TNF expression for indicated patient populations in a cohort treated with anti-PD-1 (Roh et al., 2017). Whiskers of the boxplots indicate 1.5x the interquartile ranges.
- (E) Normalized TNF signature expression (PID\_TNF\_PATHWAY, see STAR Methods) for indicated patient populations in a cohort treated with anti-PD-1 (Roh et al., 2017). Whiskers of the boxplots indicate 1.5× the interquartile ranges.
- (F) Analysis of the response duration in an ipilimumab-treated cohort (Snyder et al., 2014) as a function of the mutational status of the TNF pathway in samples that were obtained before (Pre) or after (Post) onset of anti-CTLA-4 treatment.
- (G) Using cohort from (E) but representing overall survival in a Kaplan-Meier plot. A log rank test was performed to calculate the p value.  $^*p < 0.05$ ;  $^{**}p < 0.01$ ;  $^{***}p < 0.001$ ,  $^{***}p < 0.001$ .
- See also Figure S2 and Tables S2, S3, S4, S5, S6, and S7.

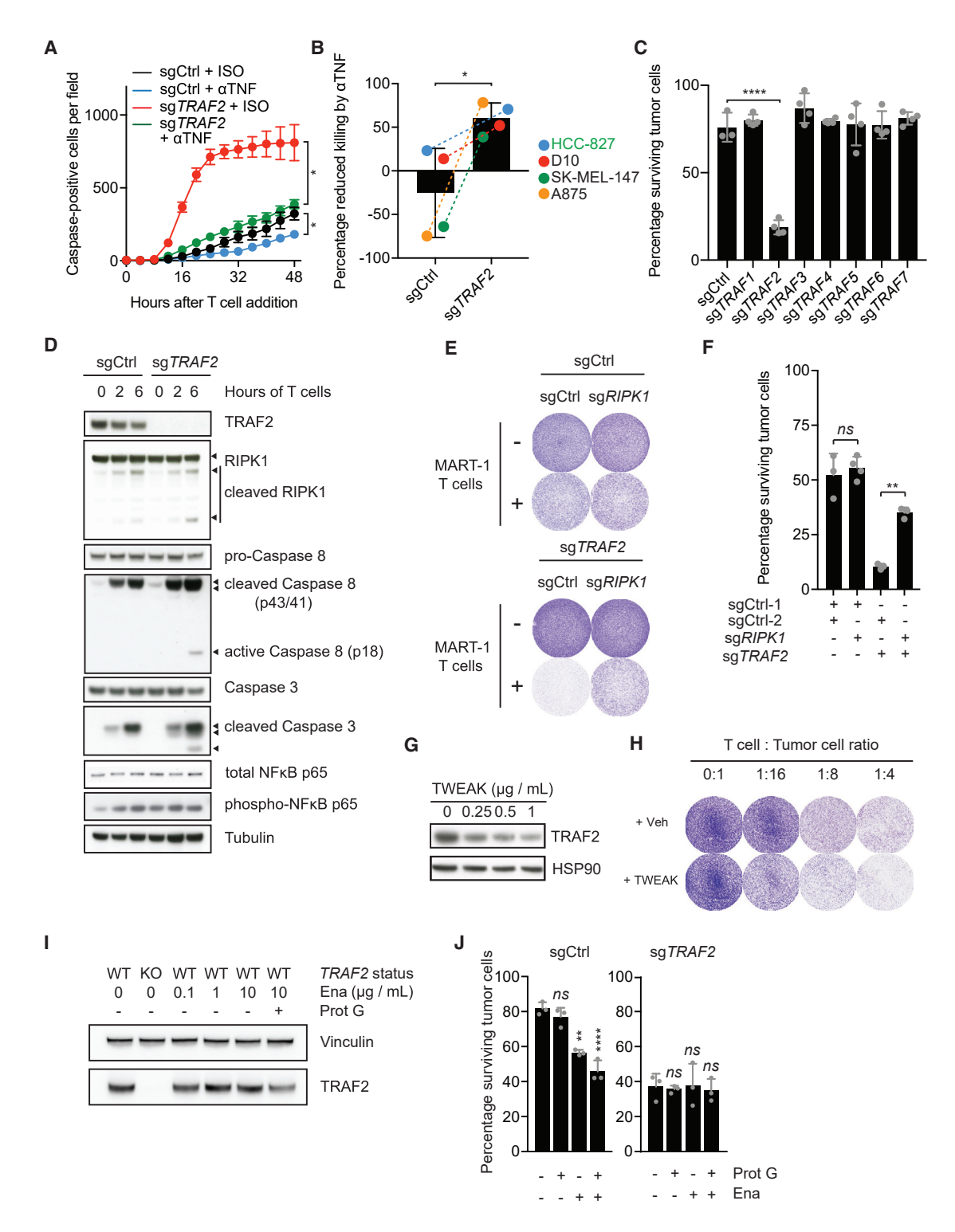


Figure 3. TRAF2 Targeting Poises Cells to Undergo RIPK1-Dependent Cell Death in Response to T Cell-Derived TNF

(A) Induction of tumor cell apoptosis as measured by a Caspase-3/7 dye in polyclonal pools of sgCtrl or sgTRAF2-transduced D10 cells after MART-1 T cell challenge in the presence or absence of a neutralizing TNF antibody (representative of 3 replicates; each n = 4). Error bars indicate SEM.

(B) As in (A), but for indicated cell lines the percentage of reduction of T cell-mediated killing (relative to ISO control) is represented. Data for each cell line is pooled for three independent replicates. Melanoma cell line names are highlighted in black text, a lung cancer cell line is highlighted in green text. Error bars indicate SD.

(C) Quantification of crystal violet staining of D10 cells harboring sgRNAs targeting indicated TRAF family members after challenge with MART-1 T cells at a 1:16 T cell: tumor cell ratio (n = 4). Error bars indicate SD.

with the clinical data described above and suggest that lowering the TNF cytotoxicity threshold, for example by TRAF2 inhibition, may benefit both untreated patients and patients who are unresponsive to ICB.

#### TRAF2 Inactivation Poises Tumors to Undergo RIPK1-Dependent Cell Death in Response to T Cell-Derived TNF

We next investigated the mechanistic interplay between T cells, TNF, and TRAF2 in more detail. First, in a T cell cytotoxicity assay, a neutralizing antibody to TNF strongly reduced T cell-induced apoptosis in *TRAF2*-deficient cells, back to the levels seen in WT melanoma cells (Figure 3A), demonstrating that TNF is the predominant T cell cytokine accounting for the TRAF2-dependent increase in susceptibility to T cell elimination. Extending this to a panel of melanoma and lung adenocarcinoma cell lines, we observed that T cell-derived TNF showed tumor cytotoxicity only after TRAF2 inactivation (Figure 3B). Among the seven TRAF family members, only the inactivation of *TRAF2* predisposed to T cell killing, suggesting a unique role for this factor (Figure 3C).

Mechanistically, we observed that in TRAF2-deficient melanomas, T cells induced cleavage of receptor interacting protein kinase 1 (RIPK1) and terminal caspase 8 activation more rapidly and strongly than in control cells (Figure 3D). This sequence of events is known to lead to RIPK1-dependent cell death (Lin et al., 1999). The engagement of this mode of cell death was confirmed by the genetic inactivation of RIPK1, which largely prevented increased sensitivity to T cells in TRAF2-deficient melanomas (Figures 3E and 3F). This epistatic rescue was not observed in TRAF2-proficient cells, implying that TRAF2 acts as a critical gatekeeper for the instigation of RIPK1-dependent cell death. While baseline phosphorylation of nuclear factor κB (NF-κB) p65 was higher in TRAF2-deficient melanoma cells, after T cell challenge there was no difference between the two genotypes, consistent with earlier observations (Yeh et al., 1997). We conclude from these results together that inactivation of TRAF2 redirects the TNF signaling pathway to favor RIPK1-dependent cell death, thereby allowing T cells to kill tumor cells more efficiently.

#### Clustering of Agonistic TWEAK Receptor Antibody Sensitizes Tumors to TNF-Dependent Cell Death by Downregulating TRAF2

We set out to begin translating these findings to a more clinical setting. Whereas no small molecule inhibitor of TRAF2 is avail-

able, stimulation of Fn14 (encoded by *TNFRSF12A*) by its ligand TWEAK can lead to the lysosomal degradation of TRAF2 (Vince et al., 2008). To determine the utility of an Fn14-based strategy to degrade TRAF2, we first assessed the expression of *TNFRSF12A* in tumors and healthy tissue. We found that the expression Fn14 is generally higher in tumors than in corresponding healthy tissues (Figure S3A) and, in melanoma, this same holds true for metastatic lesions (Figure S3B). We confirmed that treatment with TWEAK led to TRAF2 degradation (Figure 3G). More importantly, the addition of TWEAK sensitized tumor cells to T cell killing (Figure 3H).

We next investigated whether this effect could be accomplished also by means of an antibody-based targeting approach, for which we used the agonistic anti-Fn14 antibody enavatuzumab (Lam et al., 2018; Salzmann et al., 2013). Treatment with enavatuzumab caused degradation of TRAF2, and this required receptor clustering by protein G (Figure 3I). More importantly, clustered Fn14 induced sensitivity to T cell cytotoxicity in two melanoma cell lines (Figures 3J and S3C). The sensitization was dependent on TRAF2, and the degree of sensitization to T cells was of similar magnitude to that observed by the sole inactivation of TRAF2 (Figure 3J). Antibody neutralization showed that enavatuzumab-mediated sensitization was dependent on T cell-derived TNF (Figure S3D). Thus, clustering of an agonistic Fn14 antibody may be a tangible means to translate our findings to a future clinical setting.

## TRAF2 Loss Sensitizes to CD8 T Cell-Derived TNF in Immune-Proficient and ACT Animal Models

We next determined whether *TRAF2* deficiency provokes tumor sensitization to T cell cytotoxicity also *in vivo*, in two independent models. In an NSG mouse model, in which either WT or *TRAF2*-deficient clonal D10 human melanoma cell lines were grafted, there was no apparent defect in tumor growth in the absence of T cell pressure (Figures 4A and 4B). In contrast, inactivation of *TRAF2* allowed for superior tumor control compared to WT tumors in those mice injected with MART-1 T cells, demonstrating the need for immune pressure for the rejection of TRAF2-deficient tumors (Figures 4A and 4B). Injection of the anti-TNF antibody infliximab revealed that this tumor control was dependent on TNF, consistent with our *in vitro* findings (Figures 4C and 4D). Also, in keeping with our clinical data, TNF had a relatively minor contribution to T cell-mediated killing of control (TRAF2-proficient) tumors (Figure 4D).

We expanded these in vivo studies by assessing the role of murine Traf2 in an immune-competent model. For this, we

<sup>(</sup>D) Western blot analysis of D10 cell lines carrying either a non-targeting control guide (sgCtrl) or a guide targeting *TRAF2* (sg*TRAF2*) after exposure to MART-1 T cells for 0, 2, or 6 h.

<sup>(</sup>E) Representative T cell cytotoxicity assay of D10 melanoma cell lines carrying combinations of non-targeting control guides (sgCtrl), a guide targeting *TRAF2* (sg*TRAF2*), and a guide targeting *RIPK1* (sg*RIPK1*) after exposure to MART-1 T cells in indicated T cell:tumor cell ratios (n = 3).

<sup>(</sup>F) Quantification of crystal violet staining in (E). Error bars indicate SD.

<sup>(</sup>G) Western blot analysis of D10 melanoma cells treated for 8 h with indicated amounts of recombinant human TWEAK.

<sup>(</sup>H) Representative T cell cytotoxicity assay of D10 melanoma cells treated with TWEAK during exposure to MART-1 T cells in indicated T cell:tumor cell ratios

<sup>(</sup>I) Western blot analysis of D10 melanoma cells treated for 8 h with indicated amounts of enavatuzumab in the presence or absence of protein G.

<sup>(</sup>J) CellTiter-Blue quantification of a T cell cytotoxicity assay in TRAF2-proficient (left panel) and TRAF2-deficient (right panel) D10 cells treated with indicated reagents at a 1:8 T cell:tumor cell ratio (n = 4). Error bars indicate SD.

 $<sup>^*</sup>p < 0.05; \ ^{**}p < 0.01; \ ^{***}p < 0.001, \ ^{****}p < 0.0001.$ 

See also Figure S3 and Table S7.

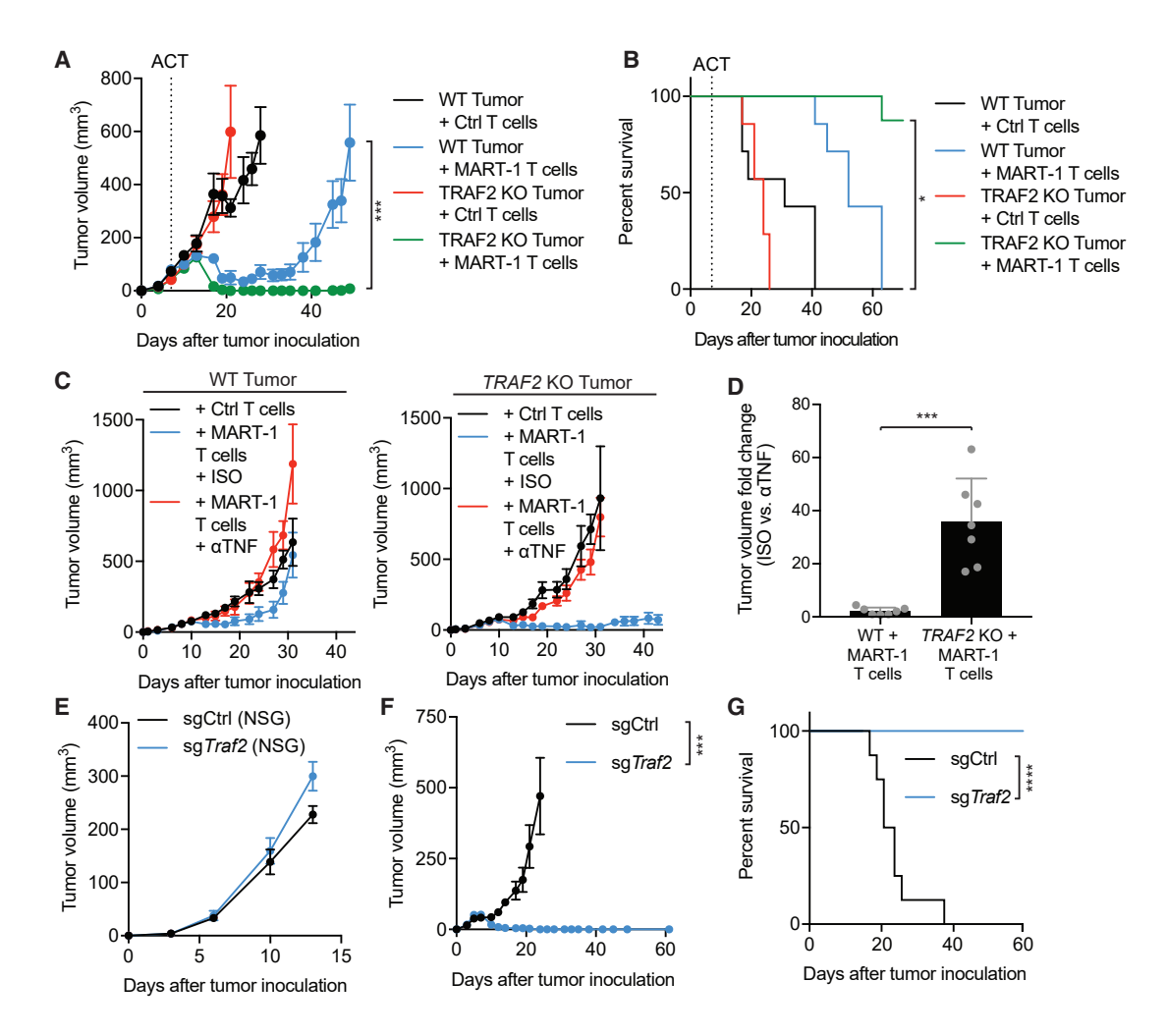


Figure 4. TRAF2 Loss Sensitizes to CD8 T Cell-Derived TNF in Immune-Proficient and ACT Animal Models

(A) In vivo growth of clonal WT and TRAF2-KO D10 cells after ACT with control or MART-1 T cells in an NSG murine xenograft model. Error bars indicate SEM; n = 8 mice per group.

- (B) Kaplan-Meier survival curves of mice from (A). Mice were sacrificed after tumors reached 500 mm<sup>3</sup>.
- (c) In vivo growth of clonal WT and TRAF2-KO D10 cells after ACT with control or MART-1 T cells, in the presence or absence of an anti-TNF antibody in an NSG murine xenograft model. Error bars indicate SEM; n = 8 mice per group.
- (D) Fold change of tumor volumes from (C). Isotype-treated mice were compared to anti-TNF-treated mice harboring clonal WT or TRAF2-KO D10 cells after ACT with control or MART-1 T cells in an NSG murine xenograft model mice. All data was normalized to the average tumor volume of isotype-treated mice in each genotype at day 30. Error bars indicate SD.
- (E) In vivo growth of polyclonal pools of sgCtrl or sgTraf2-transduced D4M.3A-OVA murine melanoma cells in NSG mice. Error bars indicate SEM; n = 10 mice per group.
- (F) In vivo growth of polyclonal pools of sgCtrl or sgTraf2-transduced D4M.3A-OVA murine melanoma cells in C57BL/6 mice. Error bars indicate SEM; n = 10 mice per group.
- (G) Kaplan-Meier survival curves of mice from (E). Mice were sacrificed after tumors reached 500 mm<sup>3</sup>. See also Figure S4 and Table S7.

injected either parental or *Traf2*-deficient D4M.3A-OVA murine melanoma cells into either C57BL/6 or NSG mice. Although all tumors initially established and grew similarly in NSG mice (Figure 4E), *Traf2*-deficient tumors were all rapidly and efficiently cleared in C57BL/6 mice, again highlighting the need for immune pressure for the clearance of *Traf2*-deficient tumors (Figure 4F). This resulted in 100% survival rates for as long as 60 days after tumor inoculation, at which time all control tumor-bearing mice had been sacrificed (Figure 4G). These results show that

TRAF2 loss strongly sensitizes to CD8 T cell-derived TNF, which allows for tumor eradication in both immunocompromised ACT and immunocompetent mouse models.

## **TRAF2** Mutations in Patients' Tumors Conferring T Cell Resistance

The mechanistic data above demonstrate that TRAF2 is a critical gatekeeper for (RIPK1-dependent) tumor cell death in response to T cell-derived TNF. Furthermore, our clinical data indicate that

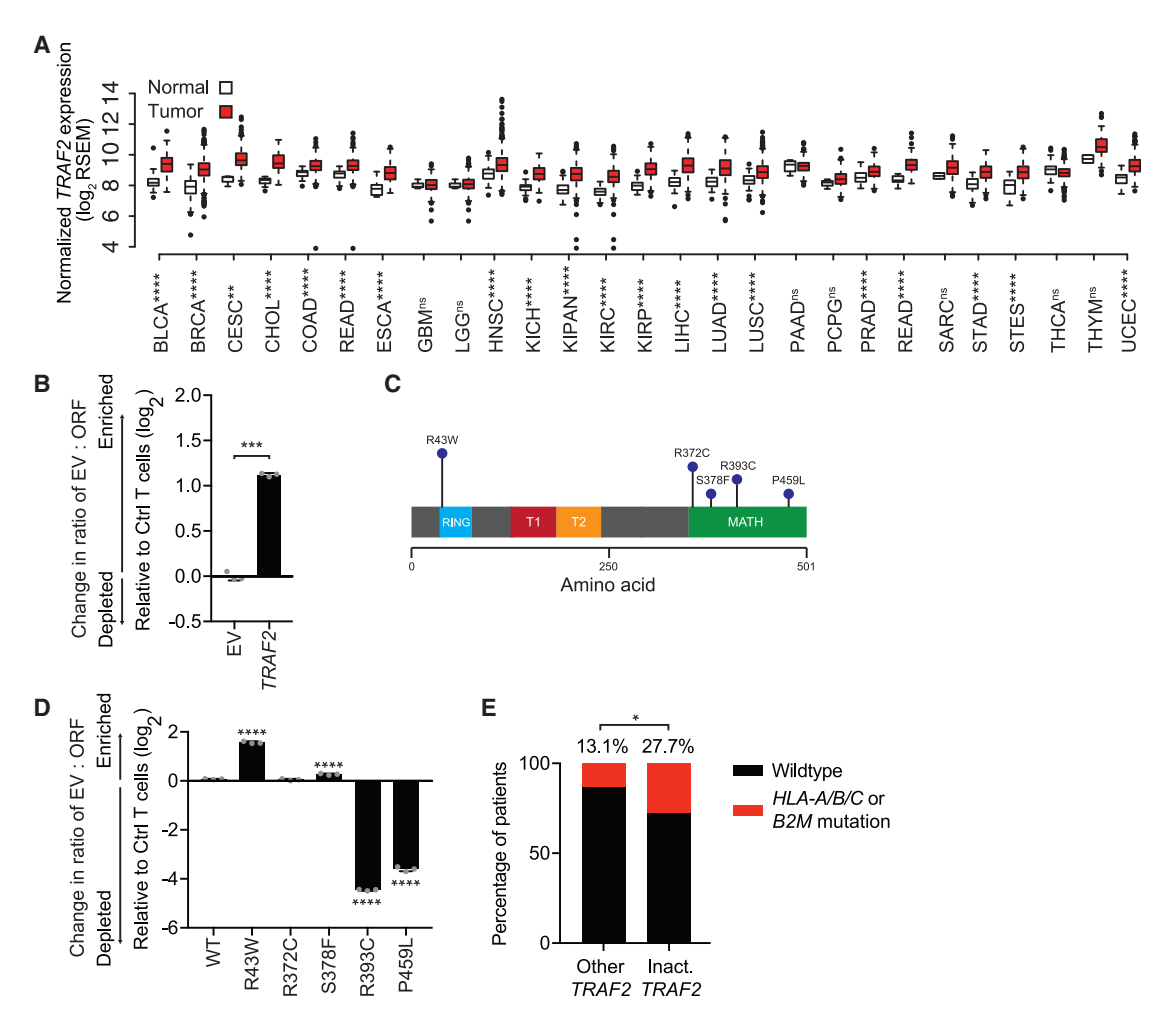


Figure 5. TRAF2 Mutations in Patients' Tumors Conferring T Cell Resistance

(A) Expression of *TRAF2* in tumor (red) and related normal tissue (white). Data are represented as  $log_2(RSEM)$  and were derived from TCGA. Whiskers of the boxplots indicate 1.5× the interquartile range.

(B) Competition assays of melanoma cells overexpressing TRAF2 or controls cells upon control or MART-1 T cell challenge. The change in ratio of cells overexpressing TRAF2 versus an empty vector control upon MART-1 T cell challenge is represented relative to melanoma cells challenged with control T cells (log<sub>2</sub>-scale). Grey dots represent individual measurements (n = 3). Error bars indicate SD.

(C) Schematic representation of the location of patient-derived mutants and functional domains in the TRAF2 protein. The length of the bar for each mutation indicates its frequency. RING, Ring finger domain; T1, TRAF type 1 domain; T2, TRAF2 type 2 domain; MATH, meprin and TRAF homology domain.

(D) Competition assays of melanoma cells expressing TRAF2 variants as indicated upon control or MART-1 T cell challenge. The change in ratio of a TRAF2 mutant versus WTTRAF2 upon MART-1 T cell challenge is represented relative to melanoma cells challenged with control T cells ( $log_2$ -scale). Grey dots represent individual measurements (n = 3). Error bars indicate SD.

(E) The relative frequency of HLA-A/B/C or B2M mutations in patients that do or do not harbor inactivating TRAF2 mutations. Significance was determined using Fisher's exact test.

 $^*p < 0.05; \ ^{**}p < 0.01; \ ^{***}p < 0.001, \ ^{****}p < 0.0001.$ 

See also Figure S4 and Table S7.

TNF expression rises with ICB response and that failure to respond to ICB correlates with mutations in the TNF pathway. Therefore, we investigated whether TRAF2 determines sensitivity to T cells in patient tumors. In the TCGA, increased expression of *TRAF2* is frequent in cancer, relative to normal tissue (Figure 5A). To determine whether such high expression levels of *TRAF2* alter the susceptibility to T cell killing, we subjected cells that ectopically express *TRAF2* to a competitive T cell cytotoxicity assay. Compared to cells with an empty vector control,

cells that overexpressed TRAF2 were more resistant to T cell killing (Figures 5B and S4A).

By mining TCGA sequencing data, we also found that *TRAF2* is recurrently mutated at a number of residues (Figure 5C). To determine whether these mutations affect T cell sensitivity, we generated tumor cell lines carrying these clinical TRAF2 mutant alleles and subjected them to a T cell cytotoxicity assay (Figure S4A). Expression of the R43W and the S378F mutants rendered melanomas more resistant to T cell killing, as judged

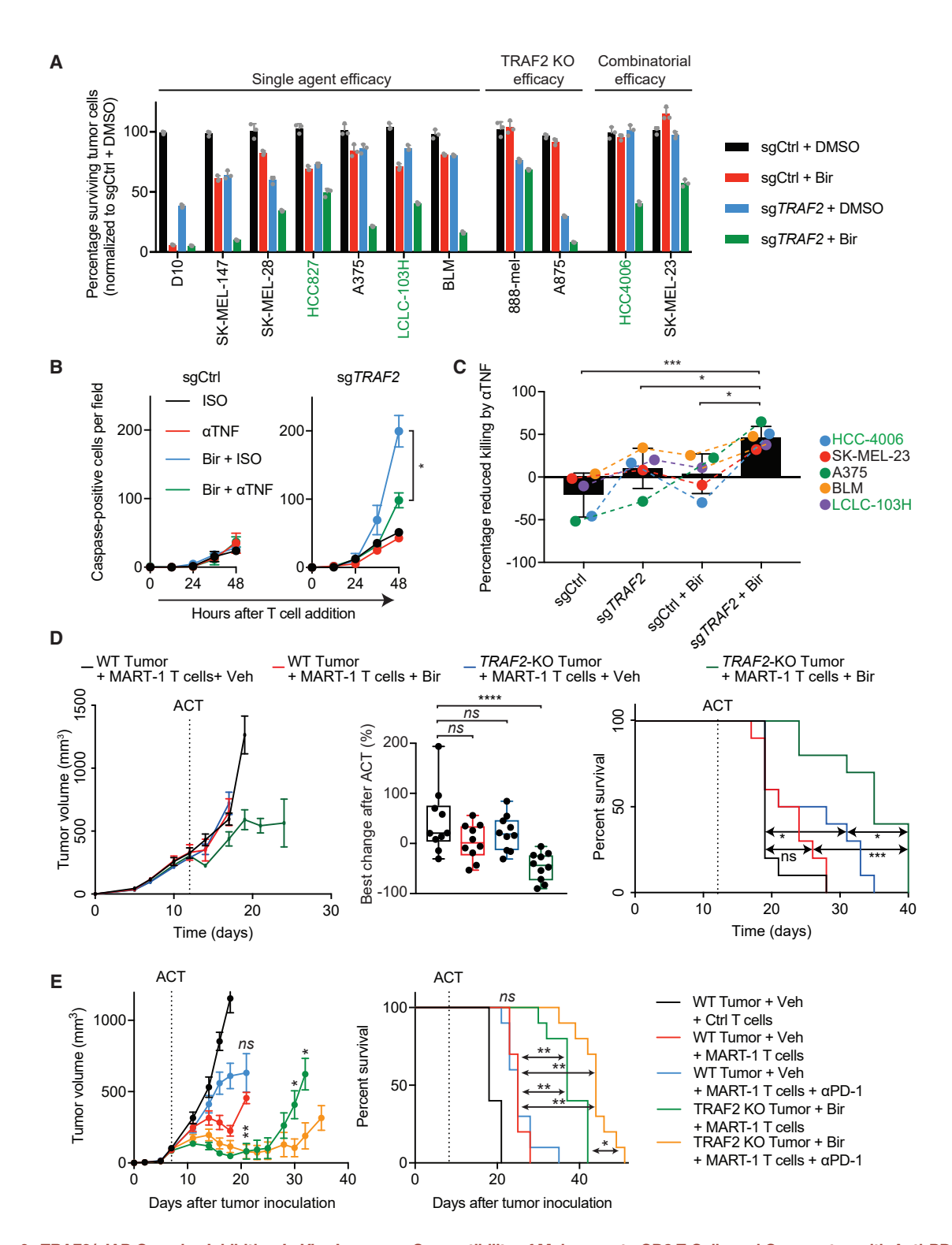


Figure 6. TRAF2/cIAP Complex Inhibition *In Vivo* Increases Susceptibility of Melanoma to CD8 T Cells and Cooperates with Anti-PD-1 (A) Tumor cell survival in MART-1 T cell cytotoxicity assays of polyclonal pools of sgCtrl or sgTRAF2-transduced melanoma (black) or lung cancer (green) cell lines in the absence or presence of birinapant. Data for all cell lines were normalized to their respective no T cell condition, and then normalized to their respective nontargeting sgRNA controls (n = 3 independent replicates). Error bars indicate SD. Tumor cell lines are subdivided in groups of single agent efficacy (significant difference in sgCtrl + DMSO versus sgCtrl + Bir or sgTRAF2 + DMSO, p < 0.001), TRAF2 KO efficacy (significant difference in sgCtrl + DMSO versus sgTRAF2 + Bir only, p < 0.001). The difference in

by both a tumor: T cell competition assay and caspase 8 signaling (Figures 5D and S3C). This observation, together with the overexpression data, suggest that patient tumors can evolve to avoid immune clearance by modulating both TRAF2 expression and function.

Two other TRAF2 mutants, R393C and P459L, instead sensitized tumor cells to T cell killing (Figure 5D). Because these mutations lie within the TRAF2 receptor-binding motif (Wu, 2004), we hypothesized that they may reduce TRAF2 incorporation into TNF receptor (TNFR) complexes, thereby hindering TRAF2 from performing its anti-apoptotic function. Indeed, TRAF2 R393C and P459L were less abundant in active TNF receptor complexes, resulting in elevated apoptotic signaling after T cell attack (Figures S4B and S4C). As our results predict it unlikely that tumors could evolve while harboring such immune-sensitizing mutations in isolation, we investigated the possible cooccurrence of compensatory genetic events. The mutation rate for both HLA I alleles or B2M was significantly higher in tumors carrying inactivating (R393, P459L, or frameshift) TRAF2 mutations than those with other TRAF2 mutations (Figure 5E). This was seen independently of general mutational load (Figure S4D). These observations suggest that tumors carrying T cell-sensitizing TRAF2 mutations are under immune-editing pressure to avoid T cell attack by, for example, loss of antigen presentation. Together, these clinical mutational data collectively imply that TRAF2 is a pivotal signaling node governing the response to T cell attack in patients' tumors.

## Combined Genetic and Pharmacologic Inhibition of TRAF2/cIAP Complex Sensitizes Panel of Melanoma and Lung Cancer Cell Lines to T Cell Killing

To study the applicability of *TRAF2* inactivation in a broader context, we inactivated this gene in a panel of 11 human melanoma and lung cancer cell lines and assessed their response to T cell exposure (Figure 6A). Cas9 targeting efficiency was high in all cell lines (Figure S5A). For nine of those, *TRAF2*-deficiency increased sensitivity to T cell killing (Figure 6A). Two tumor cell lines experienced little to no T cell sensitization, independent of their genetic makeup. We then reasoned that co-targeting another TNF pathway component may break this intrinsic T cell resistance and, reminiscent of the cooperative impact of co-inhibiting mutant BRAF and MEK in melanoma (Long et al.,

2014), may result in synergistic killing. In our CRISPR screen, we observed that aside from *TRAF2*, also loss of *BIRC2* (the second top hit, encoding cIAP1) sensitized tumor cells to T cell killing (Figure 1H). We therefore targeted *BIRC2* (or its paralog *BIRC3*) in either WT or *TRAF2*-deficient melanoma cells. In both contexts, the targeting of either *BIRC* family member resulted in increased sensitivity to T cells (Figure S5B).

Genetic loss of BIRC2/3 can be mimicked by the pharmacological drug birinapant, a bivalent SMAC mimetic degrading both BIRC2/3 protein products (Benetatos et al., 2014) (cIAP1/2, respectively; Figure S5C). Birinapant synergized with TRAF2 inactivation in inducing sensitivity to T cell killing (Figure S5D). We next tested whether co-treatment with birinapant could break T cell resistance of the tumor cell lines failing to undergo sensitization upon TRAF2 depletion. Indeed, we observed a strong synergy between TRAF2 deletion and pharmaceutical targeting of cIAP1/2 in all tested tumor cell lines, with some (e.g., SK-MEL-23) displaying increased sensitivity to T cells only in the combination setting (Figures 6A and S5E). This combinatorial approach induced a de novo sensitivity to T cell-derived TNF (Figures 6B and 6C). These data underscore the lack of efficacy of T cellderived TNF in unmanipulated tumor cells and its unleashed cytotoxic potential after selective modulation of tumor-intrinsic TNF signaling, that is, by co-inhibition of TRAF2/cIAP2.

#### TRAF2/cIAP Complex Inhibition Cooperates with Anti-PD-1 to Eliminate Tumors *In Vivo*

We set out to study any cooperative effect of the combinatorial TRAF2/cIAP targeting approach *in vivo*. For this, we selected the human melanoma cell line BLM, because of its low susceptibility to T cell killing even upon TRAF2 loss. We established both WT and *TRAF2*-deficient BLM clones and confirmed that they displayed a synergistic response to the combination of *TRAF2* deletion and cIAP1/2 inhibition *in vitro* (Figure S5F). *In vivo*, this cell line was highly resistant to ACT in our xenograft mouse model (Figures 6D and S5G). However, the combination of *TRAF2* genetic inactivation and cIAP1/2 pharmacologic inhibition by birinapant induced both a reduction in tumor volume and extended survival in these mice (Figures 6D, S5G, and S5H).

Last, we investigated whether this combinatorial targeting approach increases the efficacy of anti-PD-1 therapy. Treatment with anti-PD-1 antibodies in and of itself failed to affect rejection

sgTRAF2 + DMSO versus sgTRAF2 + Bir is significant for all cell lines (p < 0.001). Significance was determined using a one-way ANOVA with a Tukey post hoc analysis for multiple comparisons for each cell line.

(B) Induction of tumor cell apoptosis as measured by a Caspase-3/7 dye after control or MART-1 T cell attack on polyclonal pools of sgCtrl or sgTRAF2-transduced SK-MEL-23 cells in the presence or absence of a neutralizing TNF antibody and with or without birinapant (representative of 3 replicates; n = 4). Error bars indicate SEM.

(C) As in (B), but for indicated cell lines the percentage of reduction of T cell-mediated killing (relative to ISO control) is represented. Data for each cell line is pooled for three independent replicates. Melanoma cell line names are highlighted in black text, lung cancer cell line names are highlighted in green text.

(D) Left: *in vivo* growth of *TRAF2*-deficient and *TRAF2*-proficient BLM clones in an NSG murine xenograft model after ACT with MART-1 T cells in the presence of birinapant or vehicle. Error bars indicate SEM; n = 10 mice per group. Middle: best change in tumor volume after ACT in mice from left panel. If tumors were progressive, the first tumor measurement after ACT was taken as best change in tumor volume. Whiskers of the boxplots indicate 1.5× the interquartile ranges. Right: survival curves of mice from left panel. Mice were sacrificed after tumors reached 1,000 mm<sup>3</sup>.

(E) Left: *in vivo* growth of *TRAF2*-deficient and *TRAF2*-proficient BLM clones in an NSG murine xenograft model of the human BLM cell line after ACT with MART-1 T cells in the presence of birinapant or vehicle and in the presence or absence of anti-PD-1 antibodies. Right: survival curves of mice in left panel. Mice were sacrificed after tumors reached 1.000 mm<sup>3</sup>.

p < 0.05; \*\*p < 0.01; \*\*\*p < 0.001, \*\*\*\*p < 0.0001. See also Figure S5 and Table S7.

of WT tumors, confirming the relative immune resistance of this tumor cell line. In line with our clinical analyses (Figure 2D), in this non-responding setting, we failed to see an upregulation of TNF after ICB (Figure S5I). Upon treating TRAF2 KO tumors with birinapant, we observed better tumor control when compared to control tumors (Figure 6E). Moreover, when anti-PD-1 was included in this combination targeting approach, we observed superior tumor control, improving overall survival (Figure 6E). These data together imply that selective TNF pathway inhibition can leverage the antitumor activity of anti-PD-1. Furthermore, these results support the hypothesis, based on our clinical observations, that selective targeted inhibition of the TNF pathway can be explored to lower the threshold of tumor elimination by active T cells.

#### **DISCUSSION**

We report here that the TNF signaling pathway in tumor cells can be functionally mined to yield potential new immuno-oncology opportunities. We demonstrate that the tumor susceptibility threshold to TNF can be lowered by selective modulation of the TNF pathway (e.g., by TRAF2 ablation) now allowing for T cell-mediated tumor eradication. This finding is corroborated by three clinical observations. First, we analyzed several patient cohorts before and on ICB therapy. We observed that under baseline conditions, TNF is unlikely to have a strong cytotoxic effect on tumors, as neither TNF expression nor mutations in the TNF pathway have any prognostic power in that setting. Second, our data suggest that in patients responding to immunotherapy, TNF has an important role, as evidenced by the higher expression of TNF and TNF response signatures. Third, we find evidence of immune editing in the TNF pathway in ICB-treated patients, highlighting the crucial role of TNF alongside IFN $\gamma$  in T cell cytotoxicity in ICB-responsive patient tumors.

An important inference from these clinical analyses is that whereas TNF in principle has the potential to contribute to T cell-mediated tumor killing, it is hampered by its low functional pressure under baseline conditions. We confirmed this clinically observed inefficacy of TNF in several experimental models. This raises the question as to why tumors (and derived cell lines) are generally insensitive to T cell-derived TNF and, equally, TNF produced by other immune cells. Our results suggest that at least one explanation for this is that TRAF2 is commonly expressed at higher levels in tumors than in normal tissue. Consistent with this idea, we demonstrate that TRAF2 overexpression is sufficient to confer resistance to T cell cytotoxicity. Furthermore, we identified two cancer mutations in TRAF2, R43W, and S378F, which, too, render tumor cells resistant to the cytotoxic activity of TNF released by CD8 T cells. Other mechanisms by which tumor cells can escape from T cell-derived TNF, such as loss of CASP8 or TNFRSF1A, have been described in in vitro and animal models (Kearney et al., 2018).

Another important factor to consider in the context of the general inefficacy of TNF is the fact that TNF does not act only cytotoxically. Upon TNF receptor engagement, the bifurcate TNF signaling pathway can either trigger apoptosis or instead, promote cell proliferation and survival (Chen and Goeddel, 2002). Indeed, we show that some tumor cell lines experienced even a beneficial effect of T cell-derived TNF (Figures 3B and 6C). Alongside these positive effects on tumor cells, TNF has also been shown to impair mouse melanoma infiltration by CD8 T cells, and therefore anti-TNF antibodies were proposed to be used in combination with PD-1 blockade (Bertrand et al., 2017). As our data demonstrate the beneficial effects of TNF in patients who respond to ICB, we would propose to perturb tumor-intrinsic TNF signaling rather than using a neutralizing TNF antibody.

Our genome-wide CRISPR-Cas9 screen identified a number of signaling factors in the tumor-intrinsic TNF signaling cascade whose inhibition may be useful in this regard, as their inactivation led to increased sensitivity of tumors to T cell killing. As a case in point of such a clinically exploitable TNF pathway modulation, we demonstrate that TRAF2 acts as a critical mediator of both melanoma and lung cancer sensitivity to T cell-derived TNF. Patient data suggest the clinical relevance of this finding: tumors harboring inactivating mutations in TRAF2 are more likely to accumulate mutations in B2M and the HLA class I loci, implying that, also in patient tumors, loss of functional TRAF2 is likely to cause increased sensitivity to T cells. In line with this, we show that loss of TRAF2 can sensitize to clinically relevant, low levels of T cell-derived TNF. Highlighting the clinical relevance of our findings, we also find that inactivating TRAF2, in combination with birinapant, induces responses in tumors that fail to increase TNF levels upon ICB only.

To date, no small molecule inhibitors for TRAF2 are available. However, our finding that an agonistic Fn14 antibody sensitizes tumor cells to T cell-derived TNF in a TRAF2-dependent manner merits the pre-clinical optimization, which ought to include a clustering strategy, of such an antibody approach to determine its clinical feasibility in an immunotherapeutic context. Additionally, the interaction partner of TRAF2, cIAP1/2, can be inhibited by the SMAC mimetic birinapant. We demonstrate that TRAF2 inactivation synergizes with, and in some cases requires, pharmacologic inhibition of cIAP1/2 to induce cooperative lethality of tumor cells as well as to break their intrinsic T cell resistance. While birinapant has shown some efficacy in preclinical models in combination with immunotherapies (Beug et al., 2017; Kearney et al., 2017), we demonstrate here that its true efficacy can be unleashed by combined targeting of TRAF2. Canonically, TRAF2 and cIAP1/2 are thought to signal in a linear fashion, which would predict that TRAF2 inactivation cannot enhance the effect of cIAP1/2 inactivation or birinapant treatment (Hsu et al., 1996; Mahoney et al., 2008; Shu et al., 1996; Wang et al., 1998; Yeh et al., 1997). What we find, in contrast, is that TRAF2 depletion strongly enhances the degree of tumor killing by T cells upon cIAP1/2 inhibition. This implies that TRAF2 and cIAP1/2 apparently also have distinct functions in mediating and transmitting TNF input signals. Utilizing two treatment modalities converging on the same pathway, such as combined BRAF and MEK inhibition in melanoma, has proven its utility in targeted antitumor therapy regimens (Long et al., 2014). To our knowledge, a similar approach has not yet been exploited in the field of immunotherapy, but our work provides the preclinical concept that we feel merits the development of pharmacologic intervention of the TRAF2/cIAP complex. In conclusion, clinical strategies targeting specific nodes of TNF signaling in tumor cells may thus complement those impacting on T cell functionality to develop novel avenues for immunotherapies and more commonly achieve durable clinical responses to ICB.

#### **STAR**\*METHODS

Detailed methods are provided in the online version of this paper and include the following:

- KEY RESOURCES TABLE
- LEAD CONTACT AND MATERIALS AVAILABILITY
- EXPERIMENTAL MODEL AND SUBJECT DETAILS
  - Cell lines and primary cultures
  - In vivo animal studies
- METHOD DETAILS
  - O Isolation and generation of MART-1 TCR CD8 T cells
  - O Bioinformatic and RNA sequencing analysis
  - Proteomic analyses
  - In vitro cytotoxicity assays
  - Lentiviral transductions and CRISPR-mediated knockouts
  - Flow cytometry
  - Animal studies
  - Immunoblotting
  - O Whole-genome screen
  - Competition assays
  - O Cytokine measurements
- QUANTIFICATION AND STATISTICAL ANALYSIS
  - Statistics
- DATA AND CODE AVAILABILITY
  - Data Resources

#### SUPPLEMENTAL INFORMATION

Supplemental Information can be found online at https://doi.org/10.1016/j.cell.2019.06.014.

#### **ACKNOWLEDGMENTS**

We thank the Peeper lab and Blank lab members for valuable discussions. We acknowledge Ji-Ying Song for assessing immunohistochemical stainings on murine tissue, Olaf van Tellingen for help with birinapant experiments, and Alwin Huitema for providing reagents. We would like to thank the NKI-AVL Flow Cytometry Facility, Animal Laboratory Facility, Sequencing Core Facility, Animal Pathology and High-Performance Computing Facility (HPC). This work was supported by the Netherlands Organization for Scientific Research (NWO) through a VIDI grant (723.012.102) and Proteins@Work, a program of the National Roadmap Large-scale Research Facilities of the Netherlands (184.032.201 to K.E.S. and M.A.), the Dutch Cancer Society (NKI 2014-7241 to D.S.P.), the European Research Council under the European Union's Seventh Framework Programme (FP7/2007–2013)/ERC synergy (grant agreement 319661 COMBATCANCER to D.S.P.).

#### **AUTHOR CONTRIBUTIONS**

D.W.V., T.K., and D.S.P. designed and managed all experiments. D.W.V. performed the screen. T.K. and O.K. performed bioinformatics analyses. M.A.L. and J.B. designed *in vivo* experiments. M.A.L., J.B., B.d.B., and R.L. performed *in vivo* experiments. G.A. and C.U.B. contributed to *in vivo* experiments. D.W.V. and T.K. performed all other experiments. K.E.S. and M.A. were responsible for mass spectrometric analysis. X.H., J.C.N.K., R.M., R.G.-E., and T.N.S. were involved in establishing the matched tumor-T cell

system. M.Y., I.D., N.Z., and N.L.V. provided technical support. V.v.d.N. assisted with statistical analyses. D.W.V., T.K., and D.S.P. wrote the manuscript. All authors revised and approved the manuscript. The project was supervised by D.S.P.

#### **DECLARATION OF INTERESTS**

T.K. is a current employee and holder of stock options in Neogene Therapeutics. C.U.B. receives grants and/or research support from Novartis and BMS, has received honoraria or consultation fees for MSD, BMS, Roche, Novartis, GSK, Pfizer and Lilly, and is a stock shareholder of Verastem. T.N.S. is advisor for Adaptive Biotechnologies, AlMM Therapeutics, Allogene Therapeutics, Amgen, Merus, Scenic Biotech, and Neon Therapeutics, is a recipient of grant or research support from MSD, Bristol-Myers Squibb, and Merck KgaA, is a stockholder in AlMM Therapeutics, Allogene Therapeutics, Merus, Neogene Therapeutics, Scenic Biotech, and Neon Therapeutics, and is a venture partner at Third Rock Ventures. D.S.P., D.W.V., and T.K. filed the findings described in this paper for patent. The other authors declare no competing interests.

Received: May 24, 2018 Revised: January 23, 2019 Accepted: June 7, 2019 Published: July 11, 2019

#### **REFERENCES**

Adzhubei, I., Jordan, D.M., and Sunyaev, S.R. (2013). Predicting Functional Effect of Human Missense Mutations Using PolyPhen-2. Curr. Protoc. Hum. Genet. 76, 7.20.1–7.20.41.

Ahmadzadeh, M., Johnson, L.A., Heemskerk, B., Wunderlich, J.R., Dudley, M.E., White, D.E., and Rosenberg, S.A. (2009). Tumor antigen-specific CD8 T cells infiltrating the tumor express high levels of PD-1 and are functionally impaired. Blood *114*, 1537–1544.

Ayers, M., Lunceford, J., Nebozhyn, M., Murphy, E., Loboda, A., Kaufman, D.R., Albright, A., Cheng, J.D., Kang, S.P., Shankaran, V., et al. (2017). IFN-γ-related mRNA profile predicts clinical response to PD-1 blockade. J. Clin. Invest. *127*, 2930–2940.

Barber, D.L., Wherry, E.J., Masopust, D., Zhu, B., Allison, J.P., Sharpe, A.H., Freeman, G.J., and Ahmed, R. (2006). Restoring function in exhausted CD8 T cells during chronic viral infection. Nature *439*, 682–687.

Barth, R.J., Jr., Mulé, J.J., Spiess, P.J., and Rosenberg, S.A. (1991). Interferon gamma and tumor necrosis factor have a role in tumor regressions mediated by murine CD8+ tumor-infiltrating lymphocytes. J. Exp. Med. *173*, 647–658.

Benci, J.L., Xu, B., Qiu, Y., Wu, T.J., Dada, H., Twyman-Saint Victor, C., Cucolo, L., Lee, D.S.M., Pauken, K.E., Huang, A.C., et al. (2016). Tumor Interferon Signaling Regulates a Multigenic Resistance Program to Immune Checkpoint Blockade. Cell *167*, 1540–1554.

Benetatos, C.A., Mitsuuchi, Y., Burns, J.M., Neiman, E.M., Condon, S.M., Yu, G., Seipel, M.E., Kapoor, G.S., Laporte, M.G., Rippin, S.R., et al. (2014). Birinapant (TL32711), a bivalent SMAC mimetic, targets TRAF2-associated cIAPs, abrogates TNF-induced NF- $\kappa$ B activation, and is active in patient-derived xenograft models. Mol. Cancer Ther. *13*, 867–879.

Bertrand, F., Montfort, A., Marcheteau, E., Imbert, C., Gilhodes, J., Filleron, T., Rochaix, P., Andrieu-Abadie, N., Levade, T., Meyer, N., et al. (2017). TNF $\alpha$  blockade overcomes resistance to anti-PD-1 in experimental melanoma. Nat. Commun. 8, 2256.

Beug, S.T., Beauregard, C.E., Healy, C., Sanda, T., St-Jean, M., Chabot, J., Walker, D.E., Mohan, A., Earl, N., Lun, X., et al. (2017). Smac mimetics synergize with immune checkpoint inhibitors to promote tumour immunity against glioblastoma. Nat. Commun. *8*, 14278.

Blomen, V.A., Májek, P., Jae, L.T., Bigenzahn, J.W., Nieuwenhuis, J., Staring, J., Sacco, R., van Diemen, F.R., Olk, N., Stukalov, A., et al. (2015). Gene essentiality and synthetic lethality in haploid human cells. Science *350*, 1092–1096.

Borghaei, H., Paz-Ares, L., Horn, L., Spigel, D.R., Steins, M., Ready, N.E., Chow, L.Q., Vokes, E.E., Felip, E., Holgado, E., et al. (2015). Nivolumab versus Docetaxel in Advanced Nonsquamous Non-Small-Cell Lung Cancer. N. Engl. J. Med. *373*, 1627–1639.

Boshuizen, J., Koopman, L.A., Krijgsman, O., Shahrabi, A., van den Heuvel, E.G., Ligtenberg, M.A., Vredevoogd, D.W., Kemper, K., Kuilman, T., Song, J.-Y., et al. (2018). Cooperative targeting of melanoma heterogeneity with an AXL antibody-drug conjugate and BRAF/MEK inhibitors. Nat. Med. *24*, 203–212

Brincks, E.L., Katewa, A., Kucaba, T.A., Griffith, T.S., and Legge, K.L. (2008). CD8 T cells utilize TRAIL to control influenza virus infection. J. Immunol. *181*, 4918–4925.

Cao, X., Pobezinskaya, Y.L., Morgan, M.J., and Liu, Z.G. (2011). The role of TRADD in TRAIL-induced apoptosis and signaling. FASEB J. 25, 1353–1358.

Chen, G., and Goeddel, D.V. (2002). TNF-R1 signaling: a beautiful pathway. Science 296, 1634–1635.

Chen, D.S., and Mellman, I. (2017). Elements of cancer immunity and the cancer-immune set point. Nature *541*, 321–330.

Colaprico, A., Silva, T.C., Olsen, C., Garofano, L., Cava, C., Garolini, D., Sabedot, T.S., Malta, T.M., Pagnotta, S.M., Castiglioni, I., et al. (2016). TCGAbiolinks: an R/Bioconductor package for integrative analysis of TCGA data. Nucleic Acids Res. 44, e71.

Curiel, T.J., Coukos, G., Zou, L., Alvarez, X., Cheng, P., Mottram, P., Evdemon-Hogan, M., Conejo-Garcia, J.R., Zhang, L., Burow, M., et al. (2004). Specific recruitment of regulatory T cells in ovarian carcinoma fosters immune privilege and predicts reduced survival. Nat. Med. *10*, 942–949.

Dong, H., Strome, S.E., Salomao, D.R., Tamura, H., Hirano, F., Flies, D.B., Roche, P.C., Lu, J., Zhu, G., Tamada, K., et al. (2002). Tumor-associated B7-H1 promotes T-cell apoptosis: a potential mechanism of immune evasion. Nat. Med. *8*, 793–800.

Freeman, G.J., Long, A.J., Iwai, Y., Bourque, K., Chernova, T., Nishimura, H., Fitz, L.J., Malenkovich, N., Okazaki, T., Byrne, M.C., et al. (2000). Engagement of the PD-1 immunoinhibitory receptor by a novel B7 family member leads to negative regulation of lymphocyte activation. J. Exp. Med. *192*, 1027–1034.

Gao, J., Shi, L.Z., Zhao, H., Chen, J., Xiong, L., He, Q., Chen, T., Roszik, J., Bernatchez, C., Woodman, S.E., et al. (2016). Loss of IFN- $\gamma$  Pathway Genes in Tumor Cells as a Mechanism of Resistance to Anti-CTLA-4 Therapy. Cell 167, 397–404.

Gomez-Eerland, R., Nuijen, B., Heemskerk, B., van Rooij, N., van den Berg, J.H., Beijnen, J.H., Uckert, W., Kvistborg, P., Schumacher, T.N., Haanen, J.B.A.G., and Jorritsma, A. (2014). Manufacture of gene-modified human T-cells with a memory stem/central memory phenotype. Hum. Gene Ther. Methods *25*, 277–287.

Hart, T., Chandrashekhar, M., Aregger, M., Steinhart, Z., Brown, K.R., MacLeod, G., Mis, M., Zimmermann, M., Fradet-Turcotte, A., Sun, S., et al. (2015). High-Resolution CRISPR Screens Reveal Fitness Genes and Genotype-Specific Cancer Liabilities. Cell *163*, 1515–1526.

Hodi, F.S., O'Day, S.J., McDermott, D.F., Weber, R.W., Sosman, J.A., Haanen, J.B., Gonzalez, R., Robert, C., Schadendorf, D., Hassel, J.C., et al. (2010). Improved survival with ipilimumab in patients with metastatic melanoma. N. Engl. J. Med. 363, 711–723.

Hsu, H., Shu, H.-B., Pan, M.-G., and Goeddel, D.V. (1996). TRADD-TRAF2 and TRADD-FADD interactions define two distinct TNF receptor 1 signal transduction pathways. Cell *84*, 299–308.

Jacquelot, N., Roberti, M.P., Enot, D.P., Rusakiewicz, S., Ternès, N., Jegou, S., Woods, D.M., Sodré, A.L., Hansen, M., Meirow, Y., et al. (2017). Predictors of responses to immune checkpoint blockade in advanced melanoma. Nat. Commun. 8, 592.

Jenkins, M.H., Steinberg, S.M., Alexander, M.P., Fisher, J.L., Ernstoff, M.S., Turk, M.J., Mullins, D.W., and Brinckerhoff, C.E. (2014). Multiple murine BRaf(V600E) melanoma cell lines with sensitivity to PLX4032. Pigment Cell Melanoma Res. 27, 495–501.

Ji, R.R., Chasalow, S.D., Wang, L., Hamid, O., Schmidt, H., Cogswell, J., Alaparthy, S., Berman, D., Jure-Kunkel, M., Siemers, N.O., et al. (2012). An immune-active tumor microenvironment favors clinical response to ipilimumab. Cancer Immunol. Immunother. *61*, 1019–1031.

Kakaradov, B., Arsenio, J., Widjaja, C.E., He, Z., Aigner, S., Metz, P.J., Yu, B., Wehrens, E.J., Lopez, J., Kim, S.H., et al. (2017). Early transcriptional and epigenetic regulation of CD8<sup>+</sup> T cell differentiation revealed by single-cell RNA sequencing. Nat. Immunol. *18*, 422–432.

Kearney, C.J., Lalaoui, N., Freeman, A.J., Ramsbottom, K.M., Silke, J., and Oliaro, J. (2017). PD-L1 and IAPs co-operate to protect tumors from cytotoxic lymphocyte-derived TNF. Cell Death Differ. *24*, 1705–1716.

Kearney, C.J., Vervoort, S.J., Hogg, S.J., Ramsbottom, K.M., Freeman, A.J., Lalaoui, N., Pijpers, L., Michie, J., Brown, K.K., Knight, D.A., et al. (2018). Tumor immune evasion arises through loss of TNF sensitivity. Sci. Immunol. 3, eaar3451.

Kim, J.Y., Lee, J.Y., Kim, D.G., Koo, G.B., Yu, J.W., and Kim, Y.S. (2011). TRADD is critical for resistance to TRAIL-induced cell death through NF-κB activation. FEBS Lett. *585*, 2144–2150.

Kurada, B.R., Li, L.C., Mulherkar, N., Subramanian, M., Prasad, K.V., and Prabhakar, B.S. (2009). MADD, a splice variant of IG20, is indispensable for MAPK activation and protection against apoptosis upon tumor necrosis factor-alpha treatment. J. Biol. Chem. 284, 13533–13541.

Lam, E.T., Eckhardt, S.G., Messersmith, W., Jimeno, A., O'Bryant, C.L., Ramanathan, R.K., Weiss, G.J., Chadha, M., Oey, A., Ding, H.T., et al. (2018). Phase I Study of Enavatuzumab, a First-in-Class Humanized Monoclonal Antibody Targeting the TWEAK Receptor, in Patients with Advanced Solid Tumors. Mol. Cancer Ther. 17, 215–221.

Larkin, J., Chiarion-Sileni, V., Gonzalez, R., Grob, J.J., Cowey, C.L., Lao, C.D., Schadendorf, D., Dummer, R., Smylie, M., Rutkowski, P., et al. (2015). Combined Nivolumab and Ipilimumab or Monotherapy in Untreated Melanoma. N. Engl. J. Med. *373*, 23–34.

Leach, D.R., Krummel, M.F., and Allison, J.P. (1996). Enhancement of anti-tumor immunity by CTLA-4 blockade. Science 271, 1734–1736.

Li, W., Xu, H., Xiao, T., Cong, L., Love, M.I., Zhang, F., Irizarry, R.A., Liu, J.S., Brown, M., and Liu, X.S. (2014). MAGeCK enables robust identification of essential genes from genome-scale CRISPR/Cas9 knockout screens. Genome Biol. *15*, 554.

Lin, Y., Devin, A., Rodriguez, Y., and Liu, Z.G. (1999). Cleavage of the death domain kinase RIP by caspase-8 prompts TNF-induced apoptosis. Genes Dev. 13, 2514–2526.

Long, G.V., Stroyakovskiy, D., Gogas, H., Levchenko, E., de Braud, F., Larkin, J., Garbe, C., Jouary, T., Hauschild, A., Grob, J.J., et al. (2014). Combined BRAF and MEK inhibition versus BRAF inhibition alone in melanoma. N. Engl. J. Med. *371*, 1877–1888.

Love, M.I., Huber, W., and Anders, S. (2014). Moderated estimation of fold change and dispersion for RNA-seq data with DESeq2. Genome Biol. 15, 550.

Mahoney, D.J., Cheung, H.H., Mrad, R.L., Plenchette, S., Simard, C., Enwere, E., Arora, V., Mak, T.W., Lacasse, E.C., Waring, J., and Korneluk, R.G. (2008). Both cIAP1 and cIAP2 regulate TNFalpha-mediated NF-kappaB activation. Proc. Natl. Acad. Sci. USA *105*, 11778–11783.

Manguso, R.T., Pope, H.W., Zimmer, M.D., Brown, F.D., Yates, K.B., Miller, B.C., Collins, N.B., Bi, K., LaFleur, M.W., Juneja, V.R., et al. (2017). In vivo CRISPR screening identifies Ptpn2 as a cancer immunotherapy target. Nature 547, 413–418.

Motzer, R.J., Escudier, B., McDermott, D.F., George, S., Hammers, H.J., Srinivas, S., Tykodi, S.S., Sosman, J.A., Procopio, G., Plimack, E.R., et al.; CheckMate 025 Investigators (2015). Nivolumab versus Everolimus in Advanced Renal-Cell Carcinoma. N. Engl. J. Med. 373, 1803–1813.

Pan, D., Kobayashi, A., Jiang, P., Ferrari de Andrade, L., Tay, R.E., Luoma, A.M., Tsoucas, D., Qiu, X., Lim, K., Rao, P., et al. (2018). A major chromatin regulator determines resistance of tumor cells to T cell-mediated killing. Science *359*, 770–775.

- Patel, S.J., Sanjana, N.E., Kishton, R.J., Eidizadeh, A., Vodnala, S.K., Cam, M., Gartner, J.J., Jia, L., Steinberg, S.M., Yamamoto, T.N., et al. (2017). Identification of essential genes for cancer immunotherapy. Nature *548*, 537–542.
- Peng, D., Kryczek, I., Nagarsheth, N., Zhao, L., Wei, S., Wang, W., Sun, Y., Zhao, E., Vatan, L., Szeliga, W., et al. (2015). Epigenetic silencing of TH1-type chemokines shapes tumour immunity and immunotherapy. Nature *527*, 249–253.
- Post, H., Penning, R., Fitzpatrick, M.A., Garrigues, L.B., Wu, W., MacGillavry, H.D., Hoogenraad, C.C., Heck, A.J.R., and Altelaar, A.F.M. (2017). Robust, Sensitive, and Automated Phosphopeptide Enrichment Optimized for Low Sample Amounts Applied to Primary Hippocampal Neurons. J. Proteome Res. 16. 728–737.
- Riaz, N., Havel, J.J., Makarov, V., Desrichard, A., Urba, W.J., Sims, J.S., Hodi, F.S., Martín-Algarra, S., Mandal, R., Sharfman, W.H., et al. (2017). Tumor and Microenvironment Evolution during Immunotherapy with Nivolumab. Cell *171*, 934–949.
- Ritchie, M.E., Phipson, B., Wu, D., Hu, Y., Law, C.W., Shi, W., and Smyth, G.K. (2015). limma powers differential expression analyses for RNA-sequencing and microarray studies. Nucleic Acids Res. 43, e47.
- Robert, C., Thomas, L., Bondarenko, I., O'Day, S., Weber, J., Garbe, C., Lebbe, C., Baurain, J.F., Testori, A., Grob, J.J., et al. (2011). Ipilimumab plus dacarbazine for previously untreated metastatic melanoma. N. Engl. J. Med. *364*, 2517–2526.
- Roh, W., Chen, P.L., Reuben, A., Spencer, C.N., Prieto, P.A., Miller, J.P., Gopalakrishnan, V., Wang, F., Cooper, Z.A., Reddy, S.M., et al. (2017). Integrated molecular analysis of tumor biopsies on sequential CTLA-4 and PD-1 blockade reveals markers of response and resistance. Sci. Transl. Med. 9, eaah3560.
- Rosenberg, J.E., Hoffman-Censits, J., Powles, T., van der Heijden, M.S., Balar, A.V., Necchi, A., Dawson, N., O'Donnell, P.H., Balmanoukian, A., Loriot, Y., et al. (2016). Atezolizumab in patients with locally advanced and metastatic urothelial carcinoma who have progressed following treatment with platinumbased chemotherapy: a single-arm, multicentre, phase 2 trial. Lancet *387*, 1909–1920.
- Salzmann, S., Seher, A., Trebing, J., Weisenberger, D., Rosenthal, A., Siegmund, D., and Wajant, H. (2013). Fibroblast growth factor inducible (Fn14)-specific antibodies concomitantly display signaling pathway-specific agonistic and antagonistic activity. J. Biol. Chem. 288, 13455–13466.
- Sasi, S.P., Yan, X., Enderling, H., Park, D., Gilbert, H.-Y., Curry, C., Coleman, C., Hlatky, L., Qin, G., Kishore, R., and Goukassian, D.A. (2012). Breaking the 'harmony' of TNF- $\alpha$  signaling for cancer treatment. Oncogene *31*, 4117–4127.
- Schievella, A.R., Chen, J.H., Graham, J.R., and Lin, L.L. (1997). MADD, a novel death domain protein that interacts with the type 1 tumor necrosis factor receptor and activates mitogen-activated protein kinase. J. Biol. Chem. *272*, 12069–12075.
- Schulze-Osthoff, K., Ferrari, D., Los, M., Wesselborg, S., and Peter, M.E. (1998). Apoptosis signaling by death receptors. Eur. J. Biochem. *254*, 439–459
- Shalem, O., Sanjana, N.E., Hartenian, E., Shi, X., Scott, D.A., Mikkelson, T., Heckl, D., Ebert, B.L., Root, D.E., Doench, J.G., and Zhang, F. (2014). Genome-scale CRISPR-Cas9 knockout screening in human cells. Science 343. 84–87.
- Sharma, P., Hu-Lieskovan, S., Wargo, J.A., and Ribas, A. (2017). Primary, Adaptive, and Acquired Resistance to Cancer Immunotherapy. Cell *168*, 707–723.

- Shin, D.S., Zaretsky, J.M., Escuin-Ordinas, H., Garcia-Diaz, A., Hu-Lieskovan, S., Kalbasi, A., Grasso, C.S., Hugo, W., Sandoval, S., Torrejon, D.Y., et al. (2017). Primary Resistance to PD-1 Blockade Mediated by JAK1/2 Mutations. Cancer Discov. 7, 188–201.
- Shu, H.B., Takeuchi, M., and Goeddel, D.V. (1996). The tumor necrosis factor receptor 2 signal transducers TRAF2 and c-IAP1 are components of the tumor necrosis factor receptor 1 signaling complex. Proc. Natl. Acad. Sci. USA 93, 13973–13978.
- Snyder, A., Makarov, V., Merghoub, T., Yuan, J., Zaretsky, J.M., Desrichard, A., Walsh, L.A., Postow, M.A., Wong, P., Ho, T.S., et al. (2014). Genetic basis for clinical response to CTLA-4 blockade in melanoma. N. Engl. J. Med. *371*, 2189–2199.
- Subramanian, A., Tamayo, P., Mootha, V.K., Mukherjee, S., Ebert, B.L., Gillette, M.A., Paulovich, A., Pomeroy, S.L., Golub, T.R., Lander, E.S., and Mesirov, J.P. (2005). Gene set enrichment analysis: a knowledge-based approach for interpreting genome-wide expression profiles. Proc. Natl. Acad. Sci. USA 102, 15545–15550.
- Tyanova, S., and Cox, J. (2018). Perseus: A Bioinformatics Platform for Integrative Analysis of Proteomics Data in Cancer Research (Humana Press), pp. 133–148.
- Vince, J.E., Chau, D., Callus, B., Wong, W.W.-L., Hawkins, C.J., Schneider, P., McKinlay, M., Benetatos, C.A., Condon, S.M., Chunduru, S.K., et al. (2008). TWEAK-FN14 signaling induces lysosomal degradation of a cIAP1-TRAF2 complex to sensitize tumor cells to TNFalpha. J. Cell Biol. *182*, 171–184.
- Wang, C.Y., Mayo, M.W., Korneluk, R.G., Goeddel, D.V., and Baldwin, A.S., Jr. (1998). NF-kappaB antiapoptosis: induction of TRAF1 and TRAF2 and c-IAP1 and c-IAP2 to suppress caspase-8 activation. Science *281*, 1680–1683.
- Wang, T., Birsoy, K., Hughes, N.W., Krupczak, K.M., Post, Y., Wei, J.J., Lander, E.S., and Sabatini, D.M. (2015). Identification and characterization of essential genes in the human genome. Science *350*, 1096–1101.
- Wolchok, J.D., Chiarion-Sileni, V., Gonzalez, R., Rutkowski, P., Grob, J.-J., Cowey, C.L., Lao, C.D., Wagstaff, J., Schadendorf, D., Ferrucci, P.F., et al. (2017). Overall Survival with Combined Nivolumab and Ipilimumab in Advanced Melanoma. N. Engl. J. Med. 377, 1345–1356.
- Wu, H. (2004). Assembly of Post-Receptor Signaling Complexes for the Tumor Necrosis Factor Receptor Superfamily. In Advances in Protein Chemistry, K.C. Garcia, ed. (Elsevier), pp. 225–279.
- Yeh, W.C., Shahinian, A., Speiser, D., Kraunus, J., Billia, F., Wakeham, A., de la Pompa, J.L., Ferrick, D., Hum, B., Iscove, N., et al. (1997). Early lethality, functional NF-kappaB activation, and increased sensitivity to TNF-induced cell death in TRAF2-deficient mice. Immunity 7, 715–725.
- Young, L., Sung, J., Stacey, G., and Masters, J.R. (2010). Detection of Mycoplasma in cell cultures. Nat. Protoc. 5, 929–934.
- Yurkovetsky, Z.R., Kirkwood, J.M., Edington, H.D., Marrangoni, A.M., Velikokhatnaya, L., Winans, M.T., Gorelik, E., and Lokshin, A.E. (2007). Multiplex analysis of serum cytokines in melanoma patients treated with interferon-alpha2b. Clin. Cancer Res. *13*, 2422–2428.
- Zaretsky, J.M., Garcia-Diaz, A., Shin, D.S., Escuin-Ordinas, H., Hugo, W., Hu-Lieskovan, S., Torrejon, D.Y., Abril-Rodriguez, G., Sandoval, S., Barthly, L., et al. (2016). Mutations Associated with Acquired Resistance to PD-1 Blockade in Melanoma. N. Engl. J. Med. 375, 819–829.
- Zhang, S., Ke, X., Zeng, S., Wu, M., Lou, J., Wu, L., Huang, P., Huang, L., Wang, F., and Pan, S. (2015). Analysis of CD8+ Treg cells in patients with ovarian cancer: a possible mechanism for immune impairment. Cell. Mol. Immunol. *12*, 580–591.

#### **STAR**\***METHODS**

#### **KEY RESOURCES TABLE**

REAGENT or RESOURCE	SOURCE	IDENTIFIER
Antibodies		
CD3	eBioscience	16-0037-85; RRID:AB_468855
CD8	eBioscience	16-0289-85; RRID:AB_468927
$\alpha$ -mouse TCR $\beta$ chain	BD PharMingen	553172; RRID:AB_394684
Neutralizing TNF antibody	Cell Signaling Technology	7321; RRID:AB_10925386
Neutralizing TRAIL antibody	R&D Systems	AF375; RRID:AB_355334
Isotype for Neutralizing antibodies	Cell Signaling Technology	3900; RRID:AB_1550038
CD119	Miltenyi Biotech	130-099-921; RRID:AB_2654603
HLA-A2	BD Bioscience	551285; RRID:AB_394130
PD-L1	eBioscience	12-5983-42; RRID:AB_11042286
cIAP1	R&D Systems	AF8181; RRID:AB_2259001
cIAP2	Cell Signaling Technology	3130; RRID:AB_10693298
Caspase 3	Cell Signaling Technology	9665; RRID:AB_2069872
TRAF2	Abcam	Ab126758; RRID:AB_11145260
Cleaved Caspase 3	Cell Signaling Technology	9664; RRID:AB_2070042
Caspase 8	Cell Signaling Technology	4790; RRID:AB_10545768
Cleaved Caspase 8	Cell Signaling Technology	9748; RRID:AB_331181
RIPK1	Cell Signaling Technology	3493; RRID:AB_2305314
Vinculin	Cell Signaling Technology	4650; RRID:AB_10559207
Tubulin	Sigma	T9026; RRID:AB_477593
TNF-R1	Santa Cruz	sc-8436; RRID:AB_628377
Enavatuzumab	Creative Biolabs	TAB-178; RRID:AB_2459756
Anti-TNF	Slotervaart Hospital	Infliximab
Anti-PD-1	Slotervaart Hospital	Nivolumab
Chemicals, Peptides, and Recombinant Proteins		
Caspase-3/7 dye	Essen Bioscience	4440
TRAIL	ITK Diagnostics	4354
TNF	Peprotech	300-01A
TWEAK	Peprotech	310-06
Matrigel	Corning	356230
Captisol	CyDex Pharmaceuticals	RC-0C7-100
CFSE	Thermo Scientific	C34554
сту	Thermo Scientific	C34557
Retronectin	Takara	T100B
IL-2	Slotervaart Hospital	Proleukin
IL-7	Immunotools	11340075
IL-15	Immunotools	11340155
Lymphoprep	Stem Cell Technologies	07861
Crystal Violet	Sigma	V5265
Birinapant	MedChem Express	HY-16591
Biotin-TNF	R&D Systems	BT210
Pierce Recombinant Protein G	Thermo Scientific	21193

(Continued on next page)

Continued				
REAGENT or RESOURCE	SOURCE	IDENTIFIER		
Critical Commercial Assays				
CD8 Dynabeads	Thermo	11147D		
STR profiling kit	Promega	B9510		
0-plex TMT reagent	Thermo	90406		
Bradford Protein Assay	Bio-Rad	5000006		
SuperSignal West Dura Extended Duration Substrate	Thermo Scientific	34075		
NEBNext High Fidelity 2x PCR Master Mix	New England Biolabs	M0541L		
Pierce Streptavidin Magnetic Beads	Thermo Scientific	88816		
luman TNF Flex Set	BD Biosciences	560112		
CellTiter-Blue	Promega	G8080		
Deposited Data				
RNA sequencing Data	This paper	SRP132830		
Proteomics	This paper	ProteomeXchange: PXD008995		
Riaz anti-PD-1 cohort data (DNA)	Riaz et al., 2017	SRP095809		
Riaz anti-PD-1 cohort data (RNA)	Riaz et al., 2017	GEO: GSE91061		
Roh ICB-treated cohort (DNA)	Roh et al., 2017	phs001425.v1.p1		
Roh ICB-treated cohort (Nanostring)	Roh et al., 2017	Roh et al., 2017		
Snyder anti-CTLA-4 cohort data	Snyder et al., 2014	phs001041.v1.p1		
Experimental Models: Cell Lines	•	·		
88-mel (Exogenous HLA-A2, Exogenous MART-1)	Internal stock	RRID:CVCL 4632		
k375 (Exogenous HLA-A2, Exogenous MART-1)	Internal stock	RRID:CVCL_0132		
875 (Exogenous HLA-A2, Exogenous MART-1)	Internal stock	RRID:CVCL_4733		
BLM (Exogenous HLA-A2, Exogenous MART-1)	Internal stock	RRID:CVCL_7035		
010 (Endogenous HLA-A2, Endogenous MART-1)	Internal stock	N/A		
HCC4006 (Exogenous HLA-A2, Exogenous MART-1)	ATCC	CRL-2871; RRID:CVCL_1269		
HCC827 (Exogenous HLA-A2, Exogenous MART-1)	ATCC	CRL-2868; RRID:CVCL_2063		
CLC103-H (Exogenous HLA-A2, Exogenous MART-1)	DSMZ	ACC 284; RRID:CVCL_1375		
M026.X1.CL (Endogenous HLA-A2, Endogenous MART-1)	Internally generated	N/A		
M032.X2.CL (Endogenous HLA-A2, Endogenous MART-1)	Internally generated	N/A		
SK-MEL-147 (Exogenous HLA-A2, Exogenous MART-1)	Internal stock	RRID:CVCL 3876		
SK-MEL-147 (Exogenous HLA-A2, Exogenous MART-1)	Internal stock	RRID:CVCL_6027		
SK-MEL-28 (Exogenous HLA-A2, Exogenous MART-1)	Internal stock	RRID:CVCL_0526		
04M.3A (Endogenous H2-Kb, Exogenous OVA)	Constance Brinckerhoff	RRID:CVCL_0927		
HEK293T	Internal stock	RRID:CVCL_0063		
	internal stock	TH HD.0 VOL_0000		
Experimental Models: Organisms/Strains	The leakeon Laboraton	010000, DDIDJMOD JAV-010000		
NSG-β2M <sup>null</sup> mice	The Jackson Laboratory	010636; RRID:IMSR_JAX:010636		
C57BL/6J mice	Janvier	C57BL/6JRj		
Diigonucleotides	T1 *	T 11 07		
Sequencing Primers	This paper	Table S7		
gRNA sequences	This paper	Table S7		
Recombinant DNA				
entiCRISPR-v2	Addgene	RRID:Addgene_83480 / RRID:Addgene_52961		
osPAX	Addgene	RRID:Addgene_12260		
bMD2.G	Addgene	RRID:Addgene_12259		
entiCas9-Blast	Addgene	RRID:Addgene_52962		
GeCKO whole-genome knockout library	Addgene	100000049		

Cell 178, 585–599.e1–e7, July 25, 2019 e2

Continued			
REAGENT or RESOURCE	SOURCE	IDENTIFIER	
Software and Algorithms			
Proteome Discoverer 2.2	Thermo Scientific	OPTON-30795	
R version 3.4.2	R Core Team	https://www.R-project.org/	
DESeq2 version 1.16.1	Love et al., 2014	https://bioconductor.org/packages/ release/bioc/html/DESeq2.html	
javaGSEA version 2.2.3	Subramanian et al., 2005	http://software.broadinstitute.org/ gsea/index.jsp	
Rtoolbox version 1.3	This paper	https://github.com/PeeperLab/Rtoolbox	
TCGAbiolinks version 2.6.12	Colaprico et al., 2016	https://bioconductor.org/packages/ release/bioc/html/TCGAbiolinks.html	
Prism version 7.0c	Graphpad Software Inc.	https://www.graphpad.com/scientific-software/prism/	
Perseus version 1.5.6.0	Tyanova and Cox, 2018	http://maxquant.net/perseus/	
Limma version 3.34.3	Ritchie et al., 2015	https://bioconductor.org/packages/ release/bioc/html/limma.html	
Mageck version 0.5.6	Li et al., 2014	https://sourceforge.net/projects/mageck/	
Firebrowse		http://www.firebrowse.org/	
PolyPhen2	Adzhubei et al., 2013	http://genetics.bwh.harvard.edu/pph2/	

#### **LEAD CONTACT AND MATERIALS AVAILABILITY**

Further information and requests for resources and reagents should be directed to and will be fulfilled by the Lead Contact Daniel S. Peeper (d.peeper@nki.nl).

#### **EXPERIMENTAL MODEL AND SUBJECT DETAILS**

#### **Cell lines and primary cultures**

The BLM (male), SK-MEL-147 (female), D10 (female), SK-MEL-23 (female), SK-MEL-28 (male), A375 (female), 888-mel (female), A875 (female) and HEK293T (female) cell lines were all obtained from the Peeper laboratory cell line stock. The M032.X2.CL (male) and M026.X1.CL (male) cell lines are PDX-derived cell lines that we previously generated in-house (Boshuizen et al., 2018). The HCC827 (female) and HCC4006 (male) lung cancer cell lines were obtained from ATCC. The LCLC-103H (male) lung cancer cell line was obtained from DSMZ. The D4M.3A (male) murine melanoma cell line was a kind gift from Constance Brinckerhoff. Cell line identities were authenticated by means of STR profiling (Promega) and were regularly confirmed to be mycoplasma-free by PCR (Young et al., 2010). Human cell lines that lacked endogenous HLA-A\*02:01 or MART-1 expression were transduced with lentiviral constructs encoding the corresponding cDNAs. D4M.3A was modified to express the ovalbumin antigen by lentiviral transduction. All cell lines were maintained in DMEM (GIBCO) containing 9% fetal bovine serum (Sigma), 100 units per ml of penicillin and 100 μg per ml of streptomycin (both GIBCO). Primary CD8 T cells were isolated from buffycoats, which were taken from anonymous healthy donor blood (Sanquin). Both male and female donors were used. All donors gave written consent.

#### In vivo animal studies

All animal studies were approved by the animal ethics committee of the Netherlands Cancer Institute (NKI) and performed in accordance with ethical and procedural guidelines established by the NKI and Dutch legislation. Male mice, of either C57BL/6 (Janvier) or NSG-B2m (The Jackson Laboratory) mouse strains were used at an age of 8-12 weeks.

#### **METHOD DETAILS**

#### Isolation and generation of MART-1 TCR CD8 T cells

MART-1 TCR retrovirus was produced in a packaging cell line as described before (Gomez-Eerland et al., 2014). Peripheral blood mononuclear cells (PBMCs) were isolated from fresh, healthy donor buffycoats (Sanquin, Amsterdam, the Netherlands) by means of density gradient centrifugation using Lymphoprep (Stem Cell Technologies). After the PBMC fraction was isolated, CD8 T cells were purified using CD8 Dynabeads (Thermo Fisher Scientific) following manufacturer's instructions. The isolated CD8 cells were

activated for 48 hours on a 24-well plate that was pre-coated overnight with  $\alpha$ CD3 and  $\alpha$ CD28 antibodies (eBioscience, 5  $\mu$ g per well) at 2 × 10<sup>6</sup> per well. 2 × 10<sup>6</sup> Activated CD8 T cells were harvested and mixed 1:1 with MART-1 TCR retrovirus and spinfected on a Retronectin-coated (Takara, 25  $\mu$ g per well) non-tissue culture treated 24-well plate for 2 hours at 2000 g. 24 hours after spinfection, MART-1 T cells were harvested and cultured for 7 days, after which MART-1 TCR expression was confirmed by flow cytometry (BD PharMingen,  $\alpha$ -mouse TCR  $\beta$  chain). CD8 T cells were initially maintained in RPMI (GIBCO) containing 10% human serum (One Lamda), 100 units per ml of penicillin, 100  $\mu$ g per ml of streptomycin, 100 units per ml IL-2 (Proleukin, Novartis), 10ng per ml IL-7 (ImmunoTools) and 10ng per ml IL-15 (ImmunoTools). After retroviral transduction, cells were maintained in RPMI containing 10% fetal bovine serum and 100 units per ml IL-2.

#### **Bioinformatic and RNA sequencing analysis**

RNA sequencing count data were normalized and log<sub>2</sub>-transformed as log<sub>2</sub>((count + 1) per million; referred to as log<sub>2</sub>(cpm)), or using the rlog-transformation as implemented in DESeq2 (version 1.16.1) (Love et al., 2014)). For determining highly expressed cytokines (Figure S2A), a cutoff of log<sub>2</sub>(cpm) > 7 was chosen. Cytokines were filtered based on whether essential cytokine receptors were expressed (log<sub>2</sub>(cpm) > 0.1; Figures S2A–S2D). Gene set enrichment analysis (GSEA) was performed using the javaGSEA application (version 2.2.3) using the Spearman's rank correlation coefficient with T cell cytotoxicity over time as a metric for preranking, and using the C2-CP sub-collection from MSigDB (Subramanian et al., 2005) (Figures S2C and S2D). GSEA plots were redrawn using the replotGSEA function from the Rtoolbox package (https://github.com/PeeperLab/Rtoolbox). For correlation analysis on the TCGA SKCM data (Figure S2F), and to calculate expression of gene sets upon T cell co-culture (Figures S2C and S2D), log<sub>2</sub>(cpm)-values were summed for all genes in the indicated gene sets to obtain its correlation or relative expression in a given sample. For Figures 2A and 2B, log-rank p values were calculated for differences in survival based on TNF expression (1st versus 4th quartile) and on mutational status of the TNF pathway as defined by the gene set PID\_TNF\_PATHWAY. Correlation of these metrics with survival are expressed as direction (expressed as 1 for correlation or -1 for anticorrelation) \* -log10(p value). For Figures 2D, 2E, and S2G-S2J, raw read counts from RNA sequence data of patients treated with anti-PD-1 therapy were downloaded from the NCBI GEO database (GEO: GSE91061; Riaz et al., 2017). The raw read counts were normalized using the rlog-transformation as implemented in DESeq2 (version 1.16.1 (Love et al., 2014)). Normalized Nanostring data of patients with anti-PD-1 therapy were available from the supplemental data of an earlier publication (Roh et al., 2017). Differences in expression between responders (SD/PR/CR) and non-responders (PD) was assessed for TNF and PID\_TNF\_PATHWAY gene set in both datasets. The average expression levels for the PID\_TNF\_PATHWAY gene set was calculated using the z-scores for the genes from the gene set that could be matched to the available datasets. For Figures 2F and 2G, mutations in the PID\_TNF\_PATHWAY gene set were used to determine the mutational status of the TNF pathway. Analysis for Figure S2K was performed in an analogous manner as for Figure 2G, but functional effects of the mutations were first predicted by PolyPhen2. The cohort of patients was then split up per time point, and then further split into a group with no mutations or no predicted damaging mutations in the TNF pathway and in a group of patients with predicted damaging TNF pathway mutations. Only those mutations predicted to be 'probably damaging' by PolyPhen2 were assumed to be damaging. Analysis for Figure S2L were performed in an analogous manner as for Figure 2G, but for a different patient cohort (Roh et al., 2017). Only post-anti-CTLA-4 samples were assessed. Analyses for Figures S2M and S2N were performed in an analogous manner as for Figures 2F and 2G, but for mutations in the PIF\_IFNG\_PATHWAY. For the gene expression analyses in Figures S3A and 5A, healthy tissue and tumor data was downloaded from TCGA by using FireBrowse. For gene expression analysis in Figure S3B, healthy tissue and tumor data was downloaded from GTEx and TCGA databases respectively. For the proportion of HLA-A/B/C or B2M mutations in all patients and patients carrying either other or inactivating TRAF2 mutations (Figures 5E and S4D), TCGA data was used. Mutations in TRAF2 were considered inactivating when they resulted in a frameshift, or when they were either R393C or P459L. To determine significance, a Fisher exact test was performed.

#### **Proteomic analyses**

Cell pellets were lysed in a 1% sodium deoxycholate lysis buffer as described previously (Post et al., 2017). Proteins were digested overnight with Lys-C (1:75) and trypsin (1:25) at 37°C. Samples were acidified and desalted using C18 cartridges on the AssayMap BRAVO Platform (Agilent Technologies). Samples were dried and resuspended in 50mM HEPES buffer and labeled with 10-plex TMT reagent (Thermo Fisher Scientific). Labeled samples were mixed equally, desalted using Sep-Pac C18 cartridges (Waters), and fractionated on a high-pH reversed-phase C18 column (Kinetex 5u Evo C18 100A, 150 × 2.1mm, Phenomenex) coupled to an Agilent 1100 series HPLC over a 60 min gradient. For each biological replicate, fractions were concatenated to 20 fractions for proteome analysis and further pooled to 6 fractions for phosphoproteome enrichment. Phosphoproteome samples were enriched using Fe(III)-IMAC cartridges on the AssayMap BRAVO platform (Agilent Technologies) following the method described previously (Post et al., 2017). Samples were analyzed by nanoLC-MS/MS on a Q Exactive HF-X mass spectrometer (Thermo Fisher Scientific) equipped with an Agilent 1290 LC system with an LC gradient of 65 min (15% to 45% B) for proteome fractions and a 95 min gradient (9% to 35% B) for phosphoproteome fractions (Post et al., 2017). MS settings were as follows: full MS scans (375-1500 m/z) were acquired at 60,000 resolution with an AGC target of 3 × 106 charges and max injection time of 20 ms. HCD MS2 spectra were generated for the top 12 precursors using 45,000 resolution, 1 × 105 AGC target, a max injection time of 80 ms, a fixed first mass of 120 m/z, and a normalized collision energy of 32%. MS2 isolation windows were 0.7 Th for proteome samples and 1.2 Th for phosphoproteome samples. Raw data files were processed with Proteome Discover 2.2 (Thermo Fisher Scientific) using a Sequest HT search against the

Swissprot human database. Results were filtered using a 1% FDR cut-off at the protein and peptide level. TMT fragment ions were quantified using summed abundances with PSM filters requiring a S/N ≥ 10 and an isolation interference cut off of 35% or 50% (proteome or phosphoproteome). Normalized protein and peptide abundances were extracted from PD2.2 and further scaled and analyzed using Perseus software (ver. 1.5.6.0). To obtain the proteome-derived TNF signatures (Figure S2E), the limma package (version 3.34.3) (Ritchie et al., 2015) was used to determine peptides that are higher expressed in cells treated for 4 hours with TNF relative to untreated cells (adjusted p value cutoff: 0.001; adjustment method: fdr). Scaled protein and phosphopeptide abundances were median-normalized, and TNF signature expression was calculated by summing all normalized expression values of the proteins and phosphopeptides in the signature.

#### In vitro cytotoxicity assays

1.2 × 10<sup>5</sup> tumor cells were seeded per well in 12-well culture plates (Greiner). CD8 T cells were admixed in serial dilutions (two-fold, starting at a 1:1 ratio). After 24 hours, T cells were washed away. After a further 4 days, plates were fixed and stained for 1 hour using a crystal violet solution containing 0.1% crystal violet (Sigma) and 50% methanol (Honeywell). For quantification, remaining crystal violet was solubilized in 10% acetic acid (Sigma). Absorbance of this solution was measured on an Infinite 200 Pro spectrophotometer (Tecan) at 595nm. In select experiments, tumor viability data was assessed with CellTiter-Blue (Promega) following manufacturer's instructions. Where indicated, 1uM of birinapant (Selleck Chemicals) in DMSO (Sigma) was added to co-cultures. For Incucyte (Incucyte Zoom, Essen Bioscience) experiments, 5 x 10<sup>3</sup> tumor cells were seeded per well in 96-well culture plates (Greiner). CD8 T cells were admixed in indicated ratios and a Caspase-3/7 dye (Essen Bioscience) was added. Growth of these co-cultures was followed for 48 hours. When indicated, a neutralizing TNF antibody or isotype control (Cell Signaling Technology) was added at a concentration of 1 µg per ml. When indicated, enavatuzumab (indicated concentrations; Creative Biolabs) in the presence or absence of protein G (50 μg/mL; Thermo Fisher Scientific) was added. To cluster enavatuzumab, cells were pretreated for 1 hour with enavatuzumab, then protein G was added for a further 7 hours. Then, CD8 T cells were added to the tumor cells for a further 16 hours. When indicated, instead of CD8 T cells, 100ng per ml recombinant TNF (Peprotech) or recombinant TWEAK (Peprotech) at indicated concentrations was added. To perform a dose-response with TNF, 400ng/mL of TNF was added to melanoma cells as the highest dilution; this was then serially diluted in two-fold steps.

#### **Lentiviral transductions and CRISPR-mediated knockouts**

sgRNAs targeting proteins of interest were cloned into lentiCRISPR-v2 (Addgene). HEK293T cells were transfected with lentiCRISPR-v2 and the packaging plasmids psPAX and pMD2.G (both Addgene) using polyethylenimine. After 24 hours, medium was replaced by OptiMEM (GIBCO) containing 2% fetal bovine serum. 24 hours later, lentivirus-containing supernatant was harvested, filtered and stored at -80°C. For lentiviral transduction, 5 × 10<sup>5</sup> tumor cells were seeded per well in a 12-well plate (Greiner) and lentivirus was added. After 24 hours, cells were selected with antibiotics for at least 7 days. Double knockouts were generated by using both a puromycin-selectable and blasticidin-selectable variant of lentiCRISPR-v2 for each sgRNA. To establish clonal knockout cell lines, tumor cells were transfected with lentiCRISPR-v2 and clones were generated by limiting dilution or soft-agar colonies were picked. To generate IFNGR1-deficient cell lines, tumor cells were transfected with lentiCRISPR-v2 and FACSorted three times based on lack of expression of CD119 (Miltenyi Biotech). Clonal cell lines were derived from these IFNGR1-deficient cell lines by means of limiting dilution.

#### Flow cytometry

Cells were stained with antibodies targeting surface molecules of interest according to manufacturer's instructions and analyzed on a Fortessa flow cytometer (BD Bioscience). Antibodies against IFNGR1 (Miltenyi Biotech) and PD-L1 (eBioscience) were used.

#### **Animal studies**

For xenograft studies, 1 × 10<sup>6</sup> D10 or BLM human melanoma cells were admixed with Matrigel (Corning) and injected subcutaneously into NSG-β2M<sup>null</sup> mice (The Jackson Laboratory). Growth was monitored three times per week with calipers, and tumor size was calculated using the following formula: ½ × length (mm) × width (mm). When tumors reached indicated sizes, mice were randomized over different treatment groups in a blinded fashion and were inoculated with 5 x 10<sup>6</sup> human CD8 T cells, intravenously into the tail vein. In vivo persistence of T cells was stimulated by administering 100.000 U IL-2 (Proleukin, Novartis) intraperitoneally daily for three consecutive days. In selected experiments, birinapant (MedChem Express) was administered intraperitoneally once every three days. Birinipant was formulated at 3 mg/ml in 12.5% captisol (CyDex Pharmaceuticals) in water adjusted to pH 4 with hydrochloric acid. In selected experiments the TNF blocking antibody infliximab (Slotervaart Hospital) was given twice weekly (10 mg/kg). In selected experiments, the PD-1-blocking antibody nivolumab (Slotervaart Hospital) was given once weekly (5mg/kg). For studies in immunocompetent mice, 3 × 10<sup>5</sup> D4M.3A cells were injected subcutaneously into C57BL/6J mice (Janvier) and tumor growth was monitored three times per week with calipers. All experiments ended for individual mice either when the tumor volume exceeded 500 or 1000 mm<sup>3</sup>, when the tumor showed ulceration, in case of serious clinical illness, when the tumor growth blocked the movement of the mouse, or when tumor growth assessment had been completed.

#### **Immunoblotting**

Cells were lysed in RIPA buffer (50mM TRIS pH 8.0, 150mM NaCl, 1% Nonidet P40, 0.5% sodium deoxycholate, 0.1% SDS) supplemented with complete protease inhibitor cocktail (Roche Applied Science) and phosphatase inhibitors 10 mM NaF, 1 mM Na3VO4, 1 mM sodium pyrophosphate and 10 mM beta-glycerophosphate. Protein concentration was determined using a Bradford Protein Assay (Biorad). Western blotting was performed by conventional techniques using 4%-12% Bis-Tris polyacrylamide-SDS gels (Life Technologies) and nitrocellulose membranes (GE Healthcare). Blots were blocked in 4% milk powder and 0.2% Tween in PBS and then incubated overnight with primary antibodies. Western blots were then incubated in SuperSignal West Dura Extended Duration Substrate (Thermo Fisher Scientific) and luminescence was captured on high performance autoradiography films (Amersham). For co-immunoprecipitation experiments, 1x10<sup>7</sup> cells per condition were treated with 100ng/mL biotin-labeled TNF (R&D Systems) or unlabeled TNF (Peprotech) for 10 minutes. Cells were then harvested and lysed in IP lysis buffer (30mM Tris-HCl pH 7.4, 120mM NaCl, 2mM EDTA, 2mM KCl, 1% Triton X-100 and supplemented with complete protease inhibitor cocktail). Active TNF receptor complexes were then precipitated by means of streptavidin-coated magnetic beads (Thermo Fisher Scientific) for 1 hour at 4°C. Precipitate was eluted from the beads by boiling at 95°C in 1x LDS sample buffer (Thermo Fisher Scientific) containing 2.5% β-mercaptoethanol. Immunoblotting was then performed as per above. Primary antibodies against cIAP1 (R&D Systems), cIAP2 (Cell Signaling Technology), Caspase 3 (Cell Signaling Technology), TRAF2 (Abcam), cleaved Caspase 3 (Cell Signaling Technology), Caspase 8 (Cell Signaling Technology), cleaved Caspase 8 (Cell Signaling Technology), RIPK1 (Cell Signaling Technology), Vinculin (Cell Signaling Technology), α-Tubulin (Sigma), TNF-R1 (Santa Cruz) and phospho-STAT1 (Cell Signaling Technology) were used. Horseradish peroxidase-conjugated secondary antibodies against mouse IgG (Thermo Fisher Scientific), rabbit IgG (Invitrogen) and goat IgG (Thermo Fisher Scientific) were used.

#### Whole-genome screen

An *IFNGR1*-deficient clonal D10 melanoma cell line was lentivirally transduced with lentiCas9-Blast (Addgene) and infected in duplicate at a coverage of 2000x with the GeCKO whole-genome knockout library (Addgene) at an infection rate of 30%. Three days p.i., a t = 0 library reference sample was taken. After a further 11 days of puromycin (1 µg per ml; Sigma) selection, each replicate was treated with either control T cells or MART-1 T cells. Each replicate was treated with CD8 T cells from an independent donor. After 24 hours of co-culture, plates were washed twice with PBS (GIBCO) and medium was replaced. After a further 4 days of culture, the remaining melanoma cells were harvested. 18% and 21% of cells survived the T cell challenge in each respective replicate, indicating a coverage at time of harvesting of > 1000x. After harvesting, DNA was isolated from the melanoma cells by use of a Blood and Cell Culture MAXI kit (QIAGEN). sgRNA sequences were then amplified by PCR using NEBNext High-Fidelity 2x PCR Master Mix (New England BioLabs) and following manufacturer's instructions. The following primers were used:

Gecko Forward, 5'-AATGATACGGCGACCACCGAGATCTACACTCTTTCCCTACACGACGCTCTTCCGATCTNNNNNNGGCTTTA TATATCTTGTGGAAAGGACGAAACACC-3';

Gecko Reverse, 5'-CAAGCAGAAGACGGCATACGAGATCCGACTCGGTGCCATTTTTCAA-3'.

The stretch of N nucleotides indicates a unique 6 nucleotide barcode used to identify each sample in deep sequencing. After PCR, the amplified guide sequences were pooled equimolarly. The pooled guide sequences were then identified by deep sequencing. For this, the generated amplicons were analyzed on an Illumina HiSeq 2500 Sequencing system (Illumina). Obtained sequence reads were aligned to the Gecko A and B libraries and counts per sgRNA were generated, where reads containing mismatches in common and sgRNA sequence were excluded for analysis. Enrichment and depletion at the sgRNA and gene level were determined using the Mageck algorithm (version 0.5.6) (Li et al., 2014). To determine depletion of essential genes, the control T cell samples were compared with the t = 0 library reference samples, and a core essential gene set derived from the intersect of three essentialome studies (Blomen et al., 2015; Hart et al., 2015; Wang et al., 2015) was used to demarcate essential genes (Figure S1D). Enrichment and depletion of genes in the MART-1 T cell samples was determined relative to control T cell samples (Figures 1E and 1F). Gene set enrichment analysis was performed using the javaGSEA application (version 2.2.3, Subramanian et al., 2005) using the log<sub>10</sub>-transformed negative RRA score minus the log<sub>10</sub>-transformed positive score as a metric for preranking, and using the C2-CP sub-collection from MSigDB (Subramanian et al., 2005) (Figure S1E). GSEA plots were redrawn using the replotGSEA function from the Rtoolbox package (https://github.com/PeeperLab/Rtoolbox).

#### **Competition assays**

Cells containing guides of interest were labeled with either either the CellTrace CFSE Cell Proliferation Kit (CFSE; Thermo Fisher Scientific) or the CellTrace Violet Cell Proliferation Kit (CTV; Thermo Fisher Scientific) following manufacturer's instructions. Labeled cells were mixed in a 1:1 ratio and seeded at a density of  $4 \times 10^6$  melanoma cells per 10cm plate (Greiner). Labeled cells were then challenged once, at a 1:2 ratio, or three times, at a 1:8 ratio, with either MART-1 T cells or control T cells. 24 hours after the last T cell challenge, remaining melanoma cells were analyzed for CFSE and CTV staining by flow cytometry.

#### **Cytokine measurements**

Intratumoral cytokine measurements were performed using the Human TNF Flex set (BD Biosciences), generally following manufacturer's instructions, with the exception of using tumor lysate as input (1mg per sample). To prepare lysates, snap frozen tumor pieces were weighed and lysed in RIPA buffer (50mM TRIS pH 8.0, 150mM NaCl, 1% Nonidet P40, 0.5% sodium deoxycholate, 0.1% SDS) supplemented with complete protease inhibitor cocktail (Roche Applied Science) and phosphatase inhibitors 10 mM NaF, 1 mM Na3VO4, 1 mM sodium pyrophosphate and 10 mM beta-glycerophosphate. Protein concentration was determined using a Bradford Protein Assay (Biorad).

#### **QUANTIFICATION AND STATISTICAL ANALYSIS**

#### **Statistics**

To compare two means, a two-tailed Student's t test was used. To compare multiple groups of data to one control condition, we performed a one-way ANOVA, followed by a Dunnett's test to correct for multiple comparisons. For Incucyte data, selected comparisons were made by one-way ANOVA followed by Sidak multiple comparisons test. In vivo data were compared by two-tailed unpaired Student t test with Holm-Sidak multiple testing correction when data were normally distributed or by two-tailed Mann-Whitney test with Bonferroni correction for multiple comparisons when data were not normally distributed. Normality was determined by Shapiro-Wilk test. Survival analyses were performed by Log-Rank Mantel-Cox test, followed by Holm-Sidak multiple testing correction. Exceptions to these approaches are listed in the corresponding figure legends. Analyses were performed by Prism (Graphpad Software Inc., version 7.0c) or in R. Unless otherwise indicated, a P value of lower than 0.05 was regarded as being statistically significant.

#### **DATA AND CODE AVAILABILITY**

#### **Data Resources**

All data presented in this manuscript can be obtained from the short-read archive (SRA) database using accession number SRP132830. The proteomics data was submitted to ProteomeXchange under the identification number ProteomeXchange: PXD008995.

## **Supplemental Figures**

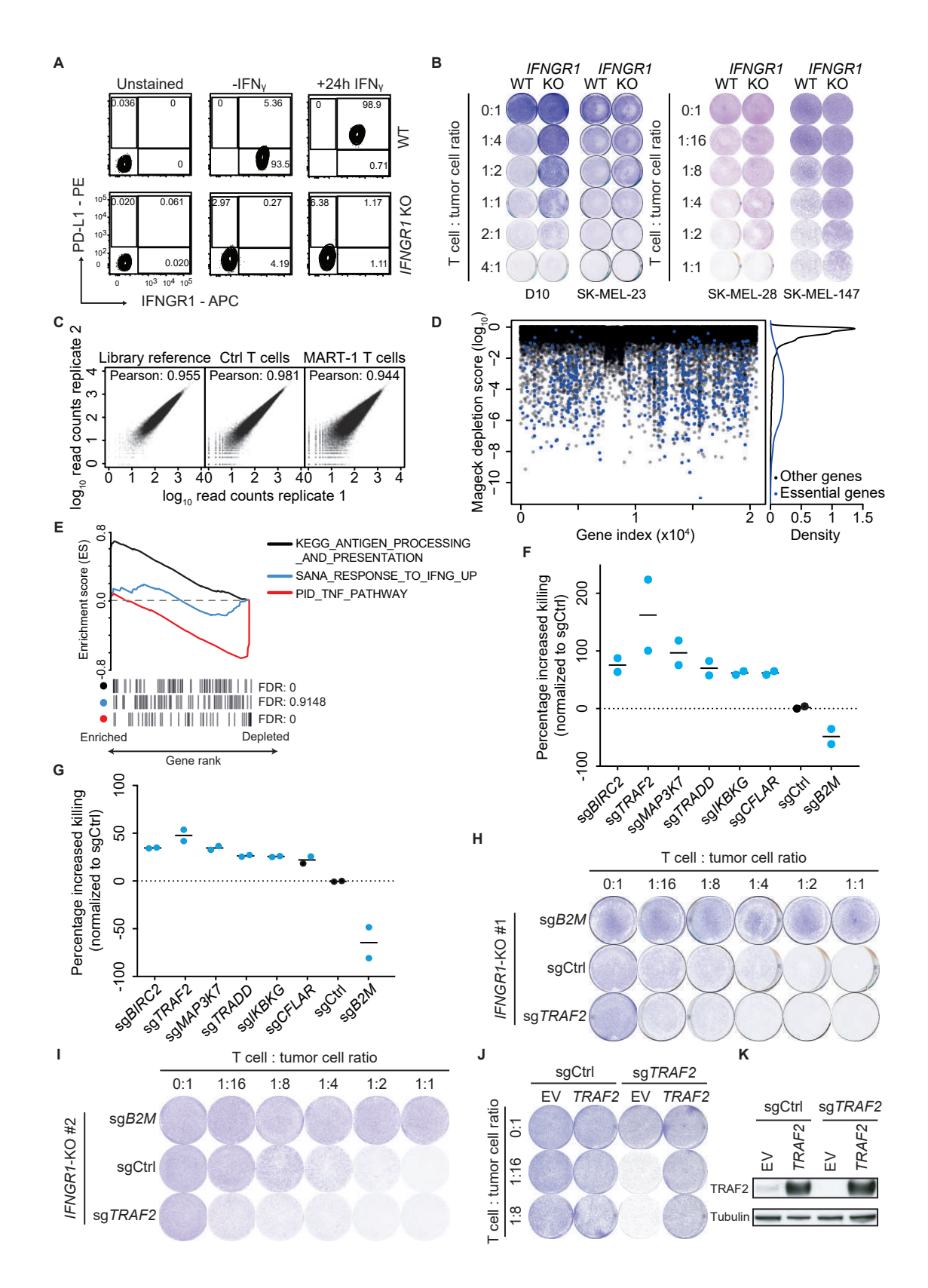


## Figure S1. Analysis and Extended Validation of Genome-wide CRISPR-Cas9 KO Screen in *IFNGR1*-Deficient Melanoma Cells, Related to Figure 1

- (A) An *IFNGR1*-deficient D10 clone was compared to wild-type melanoma cells for IFNGR1-staining and induction of PD-L1 induction upon IFN $\gamma$ -treatment (25ng/mL). Representative FACS plots of 3 independent experiments.
- (B) Representative T cell cytotoxicity assays of the indicated *IFNGR1*-proficient and *IFNGR1*-deficient human melanoma cell lines after exposure to MART-1 T cells.
- (C) Inter-replicate correlation was determined for all samples as measured by the Pearson correlation coefficient.
- (D) Log<sub>10</sub>-transformed gene-level MaGeCK RRA scores of a comparison of the control T cell-treated sample relative to the library reference control to identify essential genes. Previously identified essential genes are demarcated in blue.
- (E) Gene set enrichment analysis for the KEGG\_ANTIGEN\_PROCESSING\_AND\_PRESENTATION, SANA\_RESPONSE\_TO\_IFNG\_UP, PLASARI\_TGFB1\_TARGETS\_10HR\_UP, PID\_TNF\_PATHWAY and PID\_TRAIL\_PATHWAY genesets, based on enriched and depleted genes in Figure 1E.
- (F) Quantification of MART-1 T cell cytotoxicity assay of polyclonal pools of *IFNGR1*-KO D10 melanoma cells expressing sgCtrl or sgRNAs targeting hits. Data is normalized to the amount of killing in a non-targeting guide condition. Dots represent individual sgRNAs, and statistically significant (p < 0.05) sgRNAs are demarcated in blue (n = 4). Statistical significance was determined using a one-way ANOVA with Dunnett multiple comparisons test.
- (G) As in (F) but using an independently derived IFNGR1-KO D10 clone.
- (H) Representative images of enrichment and depletion by sgB2M and sgTRAF2 of the experiments in (F).
- (I) Representative images of enrichment and depletion by sgB2M and sgTRAF2 of the experiments in (G).
- (J) MART-1 T cell cytotoxic assay of polyclonal pools of IFNGR1-proficient D10 melanoma cells expressing sgCtrl or sgTRAF2, and which were or were not reconstituted with TRAF2. sgTRAF2 does not target the overexpression construct.

  (K) western blots of cells used in (J).
- \*p < 0.05; \*\*p < 0.01; \*\*\*p < 0.001, \*\*\*\*p < 0.0001.

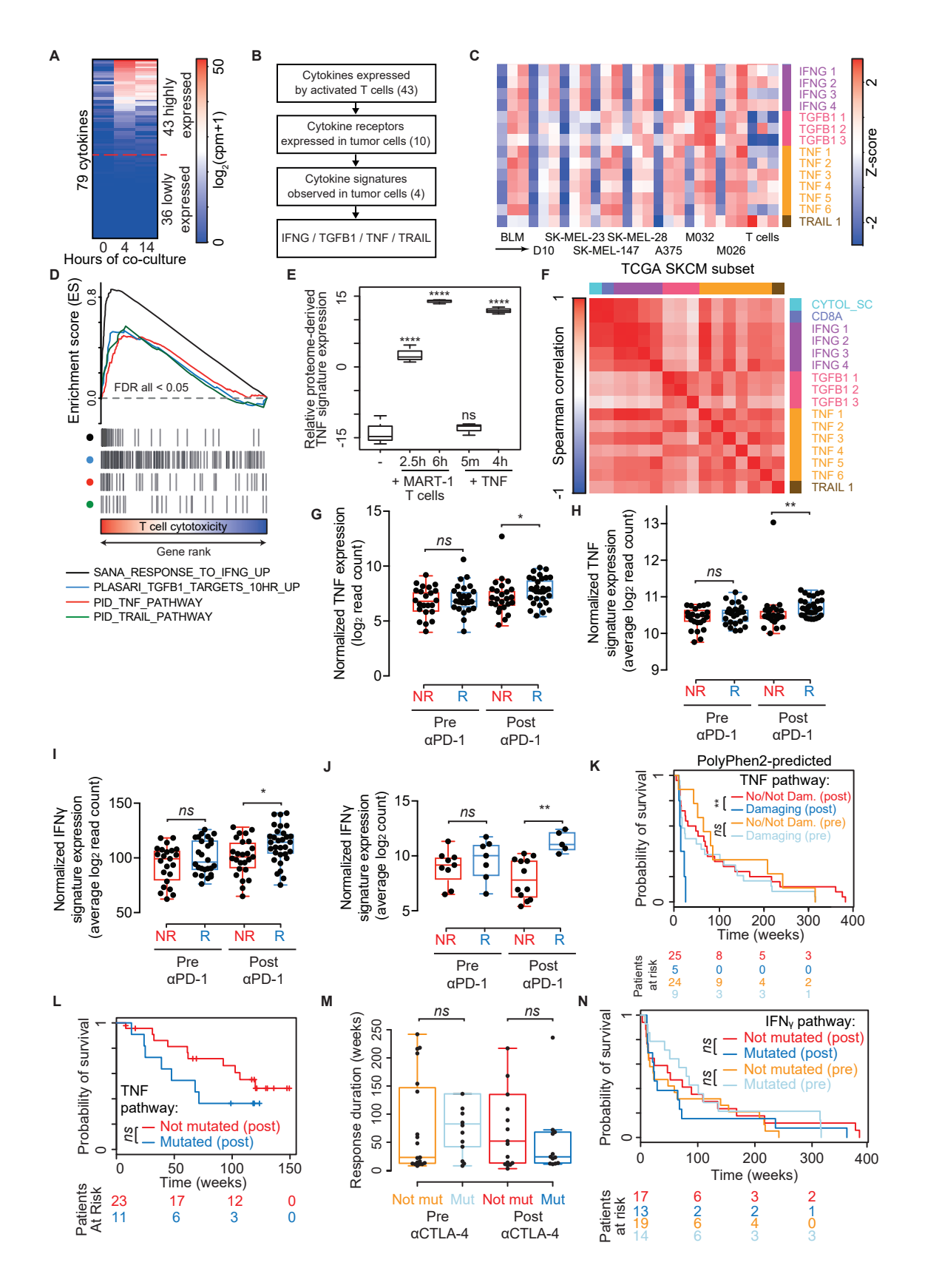


#### Figure S2. Extended Analyses Regarding the Role of TNF in Immune Responses, Related to Figure 2

- (A) RNA expression of cytokines in CD8 T cells after tumor co-culture. The dotted red line indicates the division between high and low expressed cytokines respectively. Expression is represented as log<sub>2</sub>-transformed values of normalized read counts (counts per million (cpm) + 1).
- (B) Bioinformatic flow chart for the identification of T cell derived cytokines mediating tumor cell signaling.
- (C) Expression of gene sets identified in (B) per cell line. Arrow indicates progression over time (0, 4, 14 hours of co-culture from left to right).
- (D) Gene set enrichment analysis (GSEA) plots of cytokine gene sets of samples from (B) upon MART-1 T cell challenge.
- (E) Expression of a proteome-derived TNF signature after either MART-1 T cell attack or TNF treatment as a function of time (n = 3). Whiskers of the boxplots indicate 1.5x the interquartile ranges.
- (F) Pearson correlation matrix of the expression of CD8A, cytolytic score and gene sets identified in (B) in the TCGA human skin cutaneous melanoma (SKCM) cohort.
- (G) TNF expression in a cohort of patients (Riaz et al., 2017) treated with anti-PD-1 blocking antibodies before (Pre) or after (Post) onset of therapy. Patient cohorts were split up in those responding (R) and not responding (NR) to their therapy. Significance was determined using a Mann-Whitney test to compare NR to R at each time point. Whiskers of the boxplots indicate 1.5x the interquartile ranges.
- (H) As in (G) but expression of a TNF response signature geneset (PID\_TNF\_PATHWAY, see Methods).
- (I) IFN $\gamma$  signature expression for indicated patient populations in a cohort treated with anti-PD-1 (Riaz et al., 2017). Significance was determined using a Mann-Whitney test to compare NR to R at each time point. Whiskers of the boxplots indicate 1.5x the interquartile ranges.
- (J) IFNγ signature expression for indicated patient populations in a cohort treated with anti-PD-1 (Roh et al., 2017). Significance was determined using a Student's t test to compare NR to R at each time point. Whiskers of the boxplots indicate 1.5x the interquartile ranges.
- (K) As in Figure 2G, but comparing patient cohorts with either no or no predicted damaging TNF pathway mutations versus patients with predicted damaging TNF pathway mutations.
- (L) As in Figure 2G, but for a different patient cohort (Roh et al., 2017).
- (M) As in Figure 2F, but for IFN $\gamma$  pathway mutations.
- (N) As in Figure 2G, but for IFN $\gamma$  pathway mutations.
- p < 0.05; \*p < 0.01; \*\*p < 0.001, \*\*\*p < 0.001, \*\*\*\*p < 0.0001

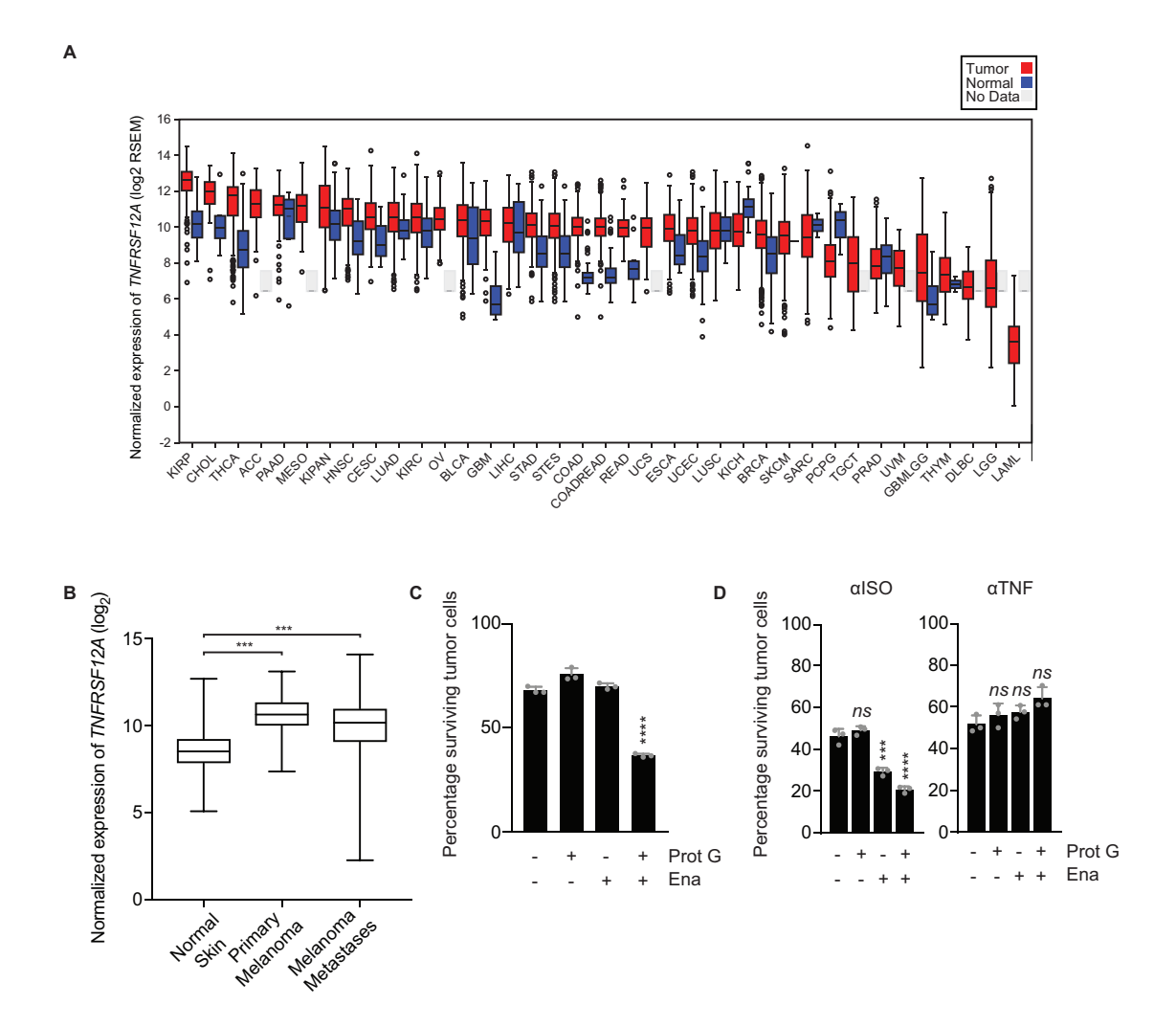


Figure S3. Clustering of Fn14-Targeted Agonistic Antibodies Sensitizes to T Cell-Derived TNF, Related to Figure 3

(A) Expression of TNFRSF12A in tumor (red) and related normal tissue (blue). Data are represented as log<sub>2</sub>(RSEM) and were derived from TCGA.

(B) Expression of TNFRSF12A in normal skin, primary melanoma and melanoma metastases. Data are represented as log<sub>2</sub>(RSEM) and were derived from GTEX and TCGA respectively. Significance was determined using a one-way ANOVA with Dunnet post hoc testing. Whiskers of the boxplots indicate minima and maxima respectively.

(C) As Figure 3J, but in TRAF2-proficient SK-MEL-147.

(D) As in Figure 3J, but in the absence (left panel) or absence (right panel) of an anti-TNF antibody and at a T cell: tumor cell ratio of 1:8.

 $^*p < 0.05;\ ^{**}p < 0.01;\ ^{***}p < 0.001,\ ^{****}p < 0.0001$ 

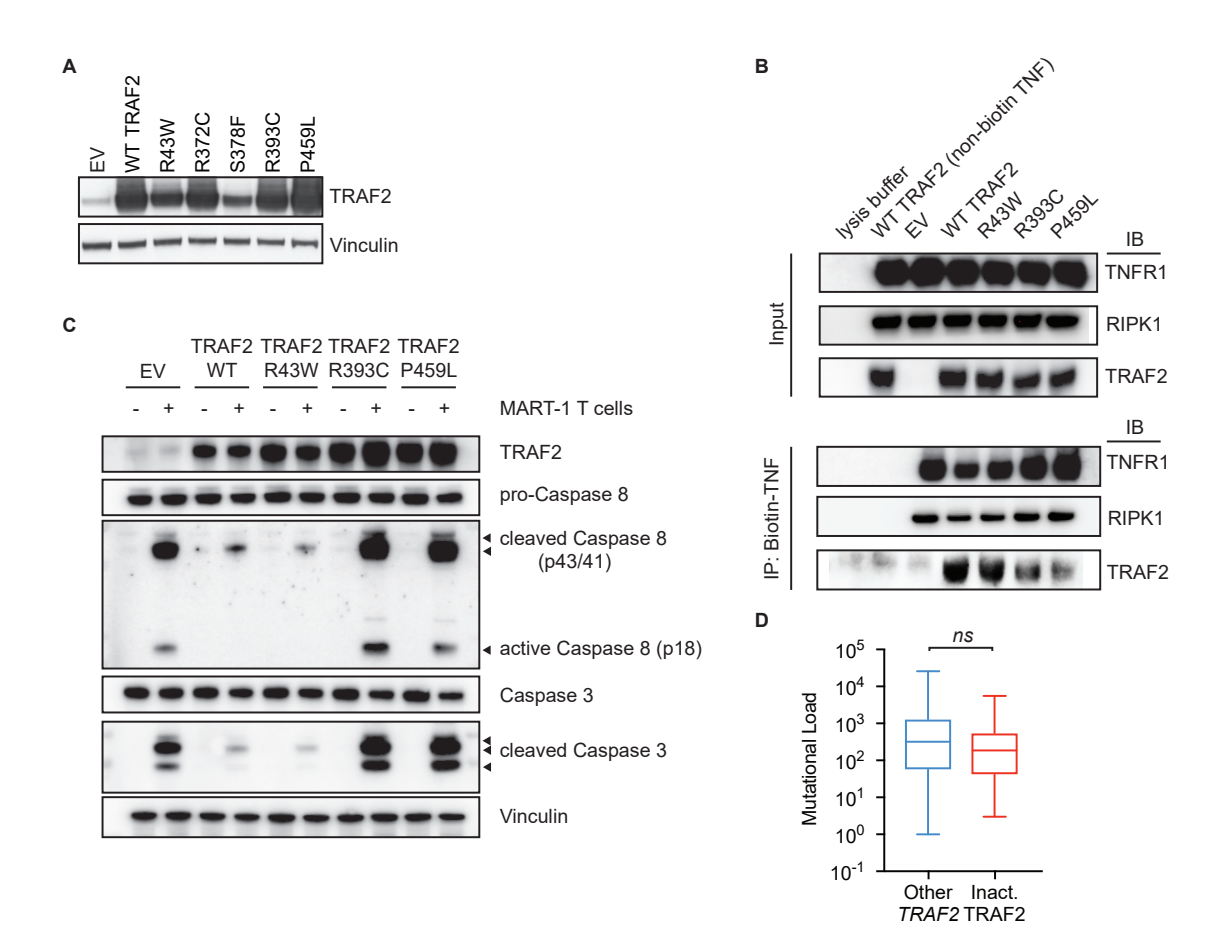


Figure S4. Extended Analyses Regarding Responses to TNF of TRAF2 Patient Variants, Related to Figure 5

(A) western blot analysis of expression of TRAF2 in cells overexpressing TRAF2 or harboring patient mutations from Figures 5B and 5D.

<sup>(</sup>B) Immunoblot of biotin-TNF co-immunoprecipitated proteins. The top panel shows the input for all samples used for the co-immunoprecipitation, the bottom panel shows the precipitated proteins.

<sup>(</sup>C) western blot analysis of cell lines used in Figure 5D after exposure to T cells, or not, for 6 hours.

<sup>(</sup>D) Mutational load of patient tumors discussed in Figure 5E. Whiskers of the boxplot indicate 1.5x the interquartile range. Significance was determined using a Mann-Whitney U test.

<sup>\*</sup>p < 0.05; \*\*p < 0.01; \*\*\*p < 0.001, \*\*\*\*p < 0.0001

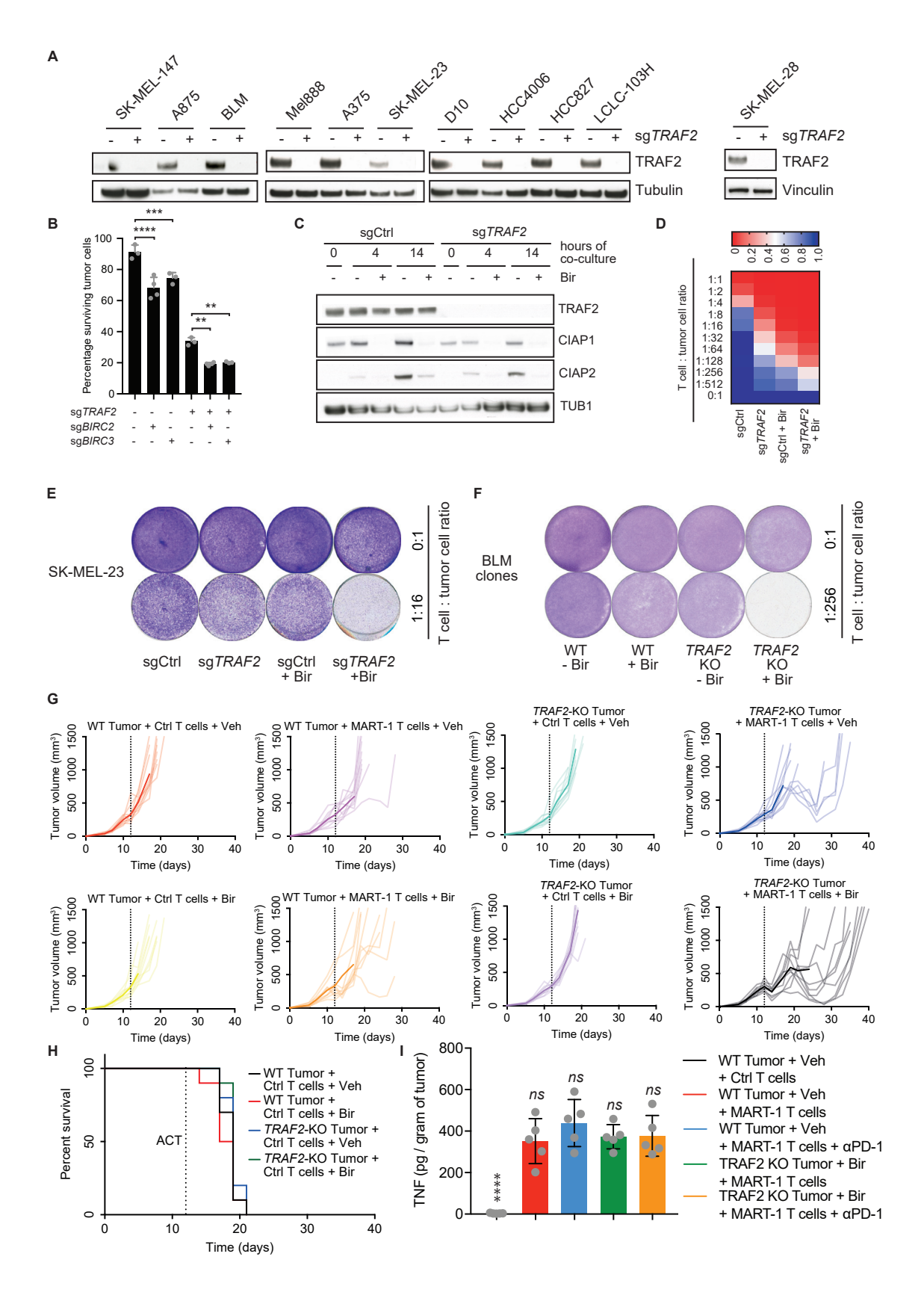


#### Figure S5. Additional Data for the Synergy between TRAF2 Inactivation and Birinapant Treatment, Related to Figure 6

- (A) western blotting of cell lines in Figure 6A to confirm successful TRAF2 targeting.
- (B) Quantification of MART-1 T cell cytotoxicity assay of polyclonal pools of D10 cells expressing sgRNAs as indicated. Error bars indicate SD (n = 4).
- (C) western blot analysis of polyclonal pools of sgCtrl or sgTRAF2-expressing SK-MEL-23 melanoma cells in the presence or absence of birinapant, and upon co-culture with MART-1 T cell for indicated amounts of time.
- (D) Quantification of MART-1 T cell cytotoxic assay of polyclonal pools of sgCtrl or sgTRAF2-transduced D10 cells with or without birinapant. All data were normalized to their respective no T cell condition (n = 3). Error bars indicate SEM.
- (E) Representative T cell cytotoxicity assay of polyclonal pools of sgCtrl or sgTRAF2-transduced SK-MEL-23 after challenge with MART-1 T cells in the presence or absence of birinapant.
- (F) Representative T cell cytotoxicity assay of a BLM WT clone and a BLM TRAF2 KO clone after challenge with MART-1 T cells in the presence or absence of birinapant.
- (G) Growth curves of the individual tumors in Figure 6D. The average is indicated in darker color, and dotted line indicates the time of ACT.
- (H) As in Figure 6D (right panel), but using control T cells.
- (I) TNF protein concentration of tumors from mice in Figure 6E. Data was normalized to tumor weight of input. Statistical significance was determined using a Kruskal-Wallis test using Tukey multiple comparison correction. Error bars indicate SD. \*p < 0.05; \*\*p < 0.01; \*\*\*p < 0.001, \*\*\*\*\*p < 0.001.

## **Update**

## Cell

Volume 180, Issue 2, 23 January 2020, Page 404–405

DOI: https://doi.org/10.1016/j.cell.2020.01.005

# Augmenting Immunotherapy Impact by Lowering Tumor TNF Cytotoxicity Threshold

David W. Vredevoogd, Thomas Kuilman, Maarten A. Ligtenberg, Julia Boshuizen, Kelly E. Stecker, Beaunelle de Bruijn, Oscar Krijgsman, Xinyao Huang, Juliana C.N. Kenski, Ruben Lacroix, Riccardo Mezzadra, Raquel Gomez-Eerland, Mete Yildiz, Ilknur Dagidir, Georgi Apriamashvili, Nordin Zandhuis, Vincent van der Noort, Nils L. Visser, Christian U. Blank, Maarten Altelaar, Ton N. Schumacher, and Daniel S. Peeper\*

\*Correspondence: d.peeper@nki.nl https://doi.org/10.1016/j.cell.2020.01.005

(Cell 178, 585-599.e1-e15; July 25, 2019)

When submitting the final high-resolution figures for publication of this article, the Tubulin panel in Figure 3D was accidentally duplicated. This error has now been corrected in the article online. This does not affect any of the conclusions of this study and the authors apologize for any inconvenience this may have caused.

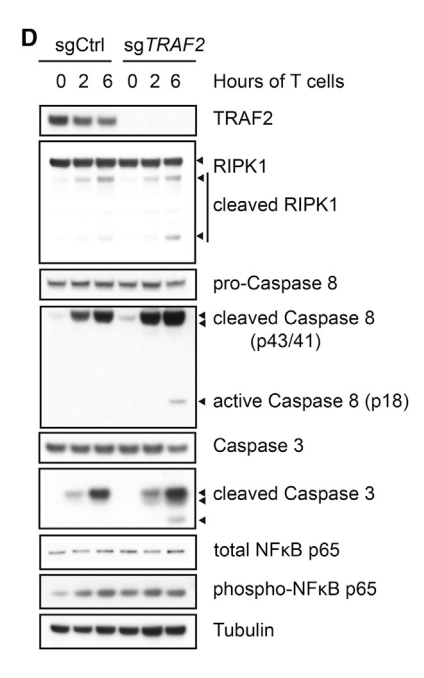


Figure 3D. TRAF2 Targeting Poises Cells to Undergo RIPK1-Dependent Cell Death in Response to T Cell-Derived TNF (corrected)
Western blot analysis of D10 cell lines carrying either a non-targeting control guide (sgCtrl) or a guide targeting TRAF2 (sgTRAF2) after exposure to MART-1 T cells for 0, 2, or 6 h.

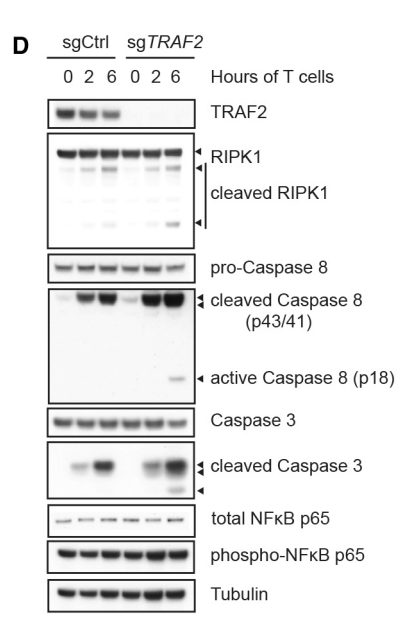


Figure 3D. TRAF2 Targeting Poises Cells to Undergo RIPK1-Dependent Cell Death in Response to T Cell-Derived TNF (original) Western blot analysis of D10 cell lines carrying either a non-targeting control guide (sgCtrl) or a guide targeting TRAF2 (sgTRAF2) after exposure to MART-1T cells for 0, 2, or 6 h.